Chaos and dynamical instability in a closed kicked system

by

Amit Anand

A thesis
presented to the University of Waterloo
in fulfillment of the
thesis requirement for the degree of
Master of Science
in
Physics (Quantum Information)

Waterloo, Ontario, Canada, 2023

Author's Declaration

This thesis consists of material all of which I authored or co-authored: see Statement of Contributions included in the thesis. This is a true copy of the thesis, including any required final revisions, as accepted by my examiners.

I understand that my thesis may be made electronically available to the public.

Statement of Contributions

Amit Anand was the sole author for Chapters 1, 2, and 5 which were written under the supervision of Dr. Shohini Ghose and were not written for publication. This thesis consists in part of two manuscripts written for publication. Exceptions to sole authorship of material are as follows:

- Chapter 3 is based on, *Simulating quantum chaos on quantum computer,* (arXiv:2107.09809v2).
  Author's Contribution : Dr. Shohini Ghose initiated the idea. Sayan Gangopadhaya and Amit Anand developed the MATLAB code for matrix decomposition. Amit Anand and Sanchit Srivastava decomposed the unitary into IBMQ gates and developed the quantum circuit. Amit Anand performed the simulations and analyzed the experimental data. All authors discussed the results. All authors prepared and revised the manuscript. Dr. Shohini Ghose supervised the project.

- Chapter 4 is based on, *Quantum recurrence in the kicked top model,* under preparation.
  Author's Contribution: Amit Anand and Dr. Shohini Ghose conceptualized the idea Amit Anand. performed the numerical simulations. Jack Davis developed the methodology. Amit Anand and Jack Davis carried out the analytical proofs and wrote the manuscript. All authors revised the manuscripts. Dr. Shohini Ghose supervised the project.

Abstract

Quantum-classical correspondence plays an important role in understanding the emergence of classical chaos from underlying quantum mechanics. However, the transition from quantum to classical is not straightforward. Here we study a well-known closed-kicked spin system with a chaotic classical limit. The quantum dynamics takes the form of stroboscopic unitary kicks acting on a single spin system. By mapping it to a programmable quantum circuit, we show that NISQ devices can be a potential testbed for simulating quantum chaos. The results suggest that entanglement can be considered a signature of classical chaos even in the deep quantum regime. Extending the work to arbitrary spins and focusing on special Hamiltonian parameters, we then show that the system may acquire temporal periodicity. These temporal periodicities do not depend on the initial state. Throughout such periodic evolutions, no initial quantum state fully explores Hilbert space as either a state vector or phase space as a quasi-probability distribution despite the classical limit being chaotic. Because these state-independent temporal periodicities are present in all dimensions, their existence represents a universal violation of the correspondence principle. We also consider the stability of this periodic behavior as a function of the degree of chaos in the classical model. Our study suggests that even in the semi-classical regime, there are specific parameter values for which a quantum system never behaves classically or displays signatures of chaos.

Acknowledgements

First of all, I would like to thank my supervisor, Prof. Shohini Ghose for giving me an opportunity to work in her group, for constant guidance and immense freedom to explore fundamental physics. Thank you for your support, for sharing your experience, and for teaching me to be critical and confident in my work. I would also like to thank my co-supervisor, Prof. Robert Mann for supporting my master's, all the discussions, and, intuitive and insightful questions during group meetings. I am deeply grateful to Prof. Alan Jamison for all the official and unofficial physics discussions. Thank you for all the valuable suggestions. It was great working under your supervision as a teaching assistant. I would also like to thank Prof. Eduardo Martin-Martinez for serving on my committee advisory and initiating exciting discussions. I would also like to thank my parents, my sisters, Ankita and Anshika, my brothers, Abhijit and Abir for all the love and caring, and support in my life. My family is the biggest reason for me being here and doing interesting science.

I would like to thank my friend and collaborator, Jack Davis and Sanchit Srivastava for their long discussions, support, and patience with me for even simple and basic things. It is great to have you both as friends. Thank you Pratyusha Chowdhury for introducing me and giving my first unofficial course on quantum information. Thanks to Tarun Agarwal, Pragati Shaw, Subhechchha Paul, Soham Chowdhury, Supratik Ghanti, Lokesh Chandra, and Supriya Pande for all the support and motivations. I would also like to thank all my friends at Waterloo, Arsalan Motamedi, Sayan Gangopadhaya, Shlok Ashok Nahar, Mannar Naeem, Omar Hussein, Mohammad Ayyash, Amolak Ratan Karla and other friends at IQC for all the scientific and non-scientific discussions. Thanks to Yash Totani and Kishore Kanddasamy for making life funny outside work. It was a great experience at IQC in last two years.

Dedication

This thesis is dedicated to my doctors, Dr. Arpita Bhattacharya, Dr. Gautam Gupta, Dr. Amol Dongre, Dr. S.D. Banavali, Dr. Dhritabrata Das, to Tata Medical Centre (Kolkata) and Tata Memorial Hospital (Mumbai) and to everyone working towards saving lives of others.

Table of Contents

List of Figures

List of Tables

Chapter 1

Introduction

> *"In the realm of chaos, where order dances with unpredictability, our quest to understand the fundamental nature of the universe unveils the delicate interplay between deterministic theory and the enigmatic dance of quantum uncertainty."*
> – ChatGPT

Since the birth of quantum physics researchers have been contemplating the question of quantum-classical transitions. The theory of chaos was completely developed on the basis of classical physics. Quantum physics and classical chaos marked two important discoveries of the twentieth century. The field of *quantum chaos* was a natural extension of the existing chaos theory. It attempts to characterize the emergence of chaotic dynamics, which is a purely classical phenomenon, from an underlying quantum substrate[1, 2]. Central to this endeavor is the notion of a *quantum-classical* correspondence, first introduced by Niels Bohr [3], which heuristically states that quantum mechanical predictions should reproduce classical predictions when the quantum numbers of the system are large enough or in certain suitable limits. While quantum-classical correspondence has been extensively explored for regular systems, limited research has been conducted in chaotic systems.

The central focus of this thesis is to explore the signatures of classical chaos in quantum systems and inspect the correspondence principle in a periodically kicked

spin system. A useful model studied in this field is the quantum kicked top (QKT) [4], a quantum system that has a well-defined *classical limit* that displays chaotic behavior. We use the tools developed in quantum information and quantum computation such as entanglement and decomposition of unitaries. We approach this problem by asking the following questions:

- Can we efficiently simulate a chaotic Hamiltonian on a quantum computer?
  We answer this question by implementing a 2-qubit QKT on IBM quantum computer and studying the overlap of quantum and classical dynamics in this model. Previous experimental implementations suffer from the systematic loss in fidelity on an increasing number of kicks or large value of the chaotic parameter (κ), see [5, 6, 7]. The current approach is resistant to the errors caused due to large number of kicks or higher values of chaoticity parameter (κ).

- Does Bohr's quantum-classical correspondence always hold in the semi-classical regime?
  To investigate this question, we show a new way of breaking quantum-classical correspondence, which is independent of system size (but finite) and initial position on the classical phase space. Previous work on breaking of Bohr's correspondence principle in QKT is shown as a result of quantum numbers or properties of the initial state in classical dynamics [8, 9].

In the remainder of the introduction, we will review the existing work in the field of quantum-classical correspondence and quantum chaos before undertaking the main study of this thesis. The results of this thesis will motivate the future experimental implementation of chaotic and other such models more coherently and will shed a new light on the relationship between classical and quantum physics.

1.1 Quantum-classical correspondence

Quantum physics has been proven successful in explaining many physical phenomena where classical theory fails to do so, such as black-body radiation, atomic spectra,

and many more [10]. It has been widely acknowledged that quantum physics as a new theory should converge with classical physics which has proven its merits over centuries, under certain suitable limits. However, in the case of chaotic systems, the predictions made by quantum theory do not always match with those of classical mechanics even in appropriate limits. Limited success has been achieved in explaining this discrepancy.

A suitable starting point for this discussion is an old theorem, proposed by Ehrenfest in 1927 [11]. The Ehrenfest correspondence theorem states that the expected evolution of quantum observables should coincide with classical trajectories up until the Ehrenfest break time (t_{Eh}), whenever the classical limit exits. In the limit of large quantum numbers, it was initially thought that t_{Eh} is very large. However, it has been shown that for chaotic systems, t_{Eh} is can be surprisingly small [12]. It is approximately equal to $\frac{1}{\lambda}\ln\left(\frac{A_o}{\hbar}\right)$, where λ is a Lyapunov exponent in classical dynamics further explained in Sec. 1.2 and A_0 is the characteristic action of the system. A simple manifestation of the above theorem was shown by Zurek and Paz [13, 14] by taking the example of Hyperion — a moon of Saturn — which is a weakly chaotic system. Using $\frac{1}{\lambda}\ln\left(\frac{A_o}{\hbar}\right)$, they calculated t_{Eh} for Hyperion to be along the order of 20 years. They argued that the correspondence in the present case is restored due to its weak coupling to the environment, which leads to decoherence.

Another line of discussion was proposed by Ford and his colleagues by studying the Arnol'd cat, where the correspondence breaks down even in the classical limit [15, 16, 17]. They considered the criterion of *algorithmic complexity* and concluded that classical chaos cannot emerge from quantum theory in the macroscopic limit. The details of the quantum-classical transitions and a better understanding of quantum manifestations of classical chaos are of considerable interest for accurate and practical descriptions of mesoscopic systems. This has led to another line of research of finding quantum signatures of classical chaos which is discussed in the next section.

1.2 Classical chaos and its quantum signatures

Classical dynamics is studied using Hamilton's equations of motion on phase space while quantum dynamics is described by the *Schrödinger* equation for states in Hilbert space. The dynamics of the Hamiltonian system with n-degrees of freedom are described on a $2n$-dimensional phase space. Hamiltonian systems can be broadly classified into two classes : *integrable* and *non-integrable* systems. A classical system with n-degrees of freedom and n independent constants of motion is said to be integrable and a system with less than n independent constants is classified as non-integrable [18].

Classical chaos is a property of non-integrable systems and is characterized by "extreme sensitivity to initial conditions"[19]. This feature is generally identified with the exponential divergence in the average separation of points initially located close to each other on phase space. The rate of separation is measured by positive Lyapunov exponents. To understand the Lyapunov exponent let's take two initial vectors, $\mathbf{X_o}$ and $\mathbf{Y_o}$, in $2n$- dimensional phase space, such that $\mathbf{Y_o} = \mathbf{X_o} + \delta_0$, where initial separation δ_o is extremely small. After time t, $\mathbf{X_o}$ and $\mathbf{Y_o}$ evolve to $\mathbf{X_t}$ and $\mathbf{Y_t}$ with δ_t being the time-dependent separation between $\mathbf{X_t}$ and $\mathbf{Y_t}$. The classical Lyapunov exponent is given by [19]

$$\lambda(\mathbf{X_o}) = \lim_{t\to\infty} \lim_{\mathbf{ffi_o}\to 0} \frac{1}{t} \ln \frac{\delta_t}{\delta_0}. \tag{1.1}$$

A strictly positive Lyapunov exponent is a signature of classical chaos.

Since there is no clear notion of "trajectories" in quantum theory, direct promotion of the classical Lyapunov exponent to a quantum one is not feasible. This has led researchers to explore different quantum properties in order to define the "quantum Lyapunov exponent" and find signatures of chaos in quantum systems. In the next part of this section, we discuss a few well-known potential signatures of chaos that have been explored in the past.

1.2.1 Fidelity decay

In the case of isolated and closed quantum systems, the evolution of quantum states is governed by unitary operators. Unitary evolution preserves the overlap of two different initial states over time. Therefore, quantum states cannot exhibit any divergence in their overlap. However, Peres proposed that instead of two different initial states, one can see the exponential divergence in overlap of same quantum states evolved with perturbed and unperturbed Hamiltonians [20]. Peres used this criteria as a signature of chaos. The overlap (F) of two states, one evolved with Hamiltonian H_o and the other with the perturbed Hamiltonian, $H_\epsilon = H_0 + \epsilon V$ is

$$F(|\psi(t)\rangle, |\psi_\epsilon\rangle) = |\langle\psi(0)| U^\dagger(t) U^\epsilon(t) |\psi(0)\rangle| \tag{1.2}$$

where U^ϵ and U correspond to time evolution unitary operator for perturbed and unperturbed Hamiltonian respectively. Shack et.al.[21] used the same concept and studied the sensitivity to random perturbations in the quantum kicked top model. They showed that if the initial state is centred in a chaotic region of the classical dynamics, it explores the large portion of the Hilbert space on evolution with the random sequence of perturbed and unperturbed Hamiltonian. On the contrary, if an initial state is centered in regular regions, then it distributes itself on Hilbert space in a localized manner. However, upon further investigation, it was shown that regular systems or systems with mixed phase show a wide variety of behaviour for fidelity decay including faster than exponential growth [22, 23]. Therefore, fidelity decay is not suitable as a universal signature of classical chaos.

1.2.2 Out-of-time-order correlators (OTOC's)

Out-of-time-order correlators were first used in the context of chaos in a thermal quantum system to give a bound on the growth of chaos [24]. It was proposed as a promising candidate for a quantum Lyapunov exponent as an analogous to classical Lyapunov exponent [25]. The out-of-time-correlator is defined as [26]

$$C(t) = -\langle [W(t), V(0)]^2 \rangle \tag{1.3}$$

where $W(t)$ and $V(0)$ are two local hermitian operators in the Heisenberg picture. Here, expectation $\langle\cdot\rangle$ is taken over any quantum state ρ of interest. It has been shown that until the Ehrenfest break time, $C(t)$ grows exponentially as $\exp^{2\tilde{\lambda}t}$, where $\tilde{\lambda}$ may be read off as a quantum Lyapunov exponent. Although $\tilde{\lambda}$ seems to be a proper quantum Lyapunov exponent, it also has a positive value for classically non-chaotic billiards [27]. It was later shown that instability in integrable quantum systems, such as Lipkin-Meshov-Glick(LMG) model [28], is sufficient for exponential growth of $C(t)$. Thus, it is unclear whether OTOC's can be used as a measure/signature of chaos.

1.2.3 Entanglement

Entanglement is a completely quantum phenomena. It does not have any classical counterpart. A bipartite quantum state, ρ^{AB} is said to be entangled if it cannot be written as

$$\rho^{AB} = \sum_{i=1}^{n} p_i \rho^A \otimes \rho^B. \tag{1.4}$$

where p_i's are non-negative real numbers and obey $\sum_{i=1}^{n} p_i = 1$, $\rho^A \in \mathcal{H}^A$ and $\rho^B \in \mathcal{H}^B$ (the Hilbert space corresponding to subsystem A and B respectively). There are different measures of entanglement such as entanglement cost, entanglement of formation, von-Neumann entropy, geometric entanglement, and distillable entanglement [29]. Some of these measures will be discussed in the background section of chapter 2. The first study of the relationship between dynamical entanglement and classically chaotic systems was done in [30]. It was followed by a series of numerical investigations of the N-atom Jaynes-Cummings model coupled to a radiation field [31, 32]. All these studies led to the broad conclusion that the rate of entanglement generation is higher for states with initial centroid in a chaotic region than the initial states centered in regular regions. The relationship between entanglement and classical dynamics has also been studied in the quantum kicked top model, both theoretically [33, 34, 35, 36, 37, 38, 9] and experimentally [7, 6, 39, 5]. A detailed discussion of these works is given in Chapter 3 and Chapter 4.

1.3 Quantum simulation

While theories provide a conceptual understanding, experiments are necessary for practical applications. Experiments not only verify the existing theory but also help to explore the new physical phenomena. In 1982, Richard Feynman pointed out the challenge of simulating quantum mechanics using classical systems [40]. He proposed that in order to accurately simulate a quantum system we need a quantum computers. This led towards a birth of the new field of quantum simulation. Quantum simulation can be loosely defined as simulating quantum systems by quantum mechanical means [41]. After more than a decade, in 1996 [42] it was shown that a quantum computer – an ensemble of well defined qubits that can be initialized, measured and acted by universal quantum gates, can act as a quantum simulator. However, a fault tolerant quantum computer that can efficiently a simulate quantum system requires a large number of qubits which is an experimental hindrance for current technologies [43, 44]. On the other hand, noisy intermediate-scale quantum (NISQ) computers already exist [43, 44].

Digital quantum simulation is one such method of simulating quantum systems using NISQ devices[43, 44]. Digital simulators decompose the unitaries corresponding to specific quantum dynamics into a set of discrete quantum gates. The set of quantum gates are implemented on quantum processor, a controlled quantum system. The quantum processor is engineered in such a way that the set of quantum gates can efficiently be implemented on it. Quantum simulation using super-conducting qubits is an example of such a quantum processor [45]. In this thesis, we show that currently available NISQ computers can be used for versatile quantum simulations of chaotic systems. The programmability of this approach allows us to experimentally explore the complete range of QKT chaoticity parameter regimes inaccessible to previous studies. Our results demonstrate the advantages of using NISQ devices for studying chaotic system over traditional experimental set-ups.

1.4 Overview

The main aim of this thesis is to study the signatures of chaos in the deep-quantum regime (small spin systems) and the transition of quantum to classical in a closed kicked spin system. We first propose a gate-based method to efficiently simulate a classically chaotic system and then undertake a study of quantum to classical transition by invoking a correspondence principle.

In chapter 2, we review the quantum kicked top model. We present its classical equations of motion and derived the unitary operator for one time period. We discuss spin-coherent states - a quantum analogue of classical states. Then we discuss the Husimi quasi-probability distribution function (or Q-function) and show how maximum value of the Q-function relates to delocalization on the spherical phase space. Finally, we discuss the different measures of entanglement used in our work such as concurrence, von Neumann entanglement entropy, and geometric entanglement.

In chapter 3, we study a quantum simulation of the quantum kicked top for $j = 1$ (2-qubits), the smallest possible system to study chaos. We first introduce the multi-qubit representation of the quantum kicked top. The qubit representation of the QKT can be considered as a symmetric multi-qubit system. We introduce a classical-quantum hybrid approach for exploring the dynamics of the chaotic quantum kicked top on a universal quantum computer. The number of gates in our simulation does not increase with the number of kicks, thus making it possible to study the QKT evolution for arbitrary number of kicks without fidelity loss. Using a publicly accessible NISQ computer (IBMQ), we observe periodicities in the evolution of the 2-qubit QKT. We then study the relationship between the entanglement and classical chaos and show that entanglement can be used as a signature of chaos even in the deep quantum regime. We demonstrate a connection between entanglement and delocalization in the 2-qubit QKT. We also reproduce the mixed-phase space of classical dynamics using time averaged entanglement.

In chapter 4, we deal with the study of the Bohr's correspondence principle for arbitrary but finite spin value. We first prove the periodicity of quantum correlations in QKT in κ, a chaoticity parameter in QKT. We then study the temporal periodicity in

the evolution of arbitrary states for some special values of the system's parameter. We analytically prove the temporal periodicity for κ of the form $mj\pi$, where m is an even integer for both integer and half-integer spin. For the case of odd values of m, we show the temporal periodicity with numerical simulations for the integer spin system. We then analyse the stability of these special parameter values using von-Neuman entropy and show that the evolutions of the states are relatively stable in time to perturbation these κ values. We also discuss the absence of temporal periodicity for $\kappa = \frac{j\pi}{2}$ and half-integer spin.

In chapter 5 we summarize the results of this thesis and discuss future work.

Chapter 2

Background

2.1 Kicked Top model

The quantum kicked top (QKT) is a finite-dimensional dynamical model used to study quantum chaos, known for its compact phase space and parameterizable chaoticity structure [4]. The time-dependent, periodically-driven system is governed by the Hamiltonian

$$H = \hbar \frac{pJ_y}{\tau} + \hbar \frac{\kappa J_z^2}{2j} \sum_{n=-\infty}^{\infty} \delta(t - n\tau), \tag{2.1}$$

where $\{J_x, J_y, J_z\}$ are the angular momentum operators: $[J_i, J_j] = i\epsilon_{ijk}J_k$. It describes a spin of size j precessing about the y-axis together with impulsive state-dependent twists about the z-axis with magnitude characterized by the chaoticity parameter κ. Here we are using a non-zero length, finite sized impulse that will converge to the delta kick as $\delta \to 0$. The period between kicks is τ, and p is the amount of y-precession within one

period. The associated Floquet time evolution operator for one period is

$$\begin{aligned} U &= e^{-\int \frac{iH}{\hbar} dt} \\ &= \lim_{\delta\tau \to 0} U(\tau, \tau - \delta\tau) U(\tau - \delta\tau, 0) \\ &= \lim_{\delta\tau \to 0} \exp\left(\frac{-i}{\hbar} \int_{\tau-\delta\tau}^{\tau} \left(\hbar \frac{p}{\tau} J_y + \hbar \frac{\kappa}{2j\delta\tau} J_z^2 \right) dt \right) \exp\left(\frac{-i}{\hbar} \int_0^{\tau-\delta\tau} (\hbar \frac{p}{\tau} J_y) dt \right) \\ &= \lim_{\delta\tau \to 0} \exp\left(-i \frac{p}{\tau} J_y \delta\tau - i \frac{\kappa}{2j} J_z^2 \right) \exp\left(-i \frac{p}{\tau} J_y (\tau - \delta\tau) \right) \\ &= \exp\left(-i \frac{\kappa}{2j} J_z^2 \right) \exp\left(-i \frac{p}{\tau} J_y \right) \end{aligned} \tag{2.2}$$

For any given initial state $|\psi(0)\rangle$, the consequent state after n kicks, $|\psi(n)\rangle$ can be obtained on applying U for n times.

The classical kicked top can be obtained by computing the Heisenberg equations for the re-scaled angular momentum, J_i/j, where $i \in \{x, y, z\}$ followed by the limit $j \to \infty$ [4]. In the commonly considered case of $(\tau = 1, p = \pi/2)$, the classical map is

$$\begin{aligned} X_{n+1} &= Z_n \cos(\kappa X_n) + Y_n \sin(\kappa X_n), \\ Y_{n+1} &= Y_n \cos(\kappa X_n) - Z_n \sin(\kappa X_n), \\ Z_{n+1} &= -X_n. \end{aligned} \tag{2.3}$$

The dynamical variable (X, Y, Z) satisfies the constraints $X^2 + Y^2 + Z^2 = 1$, i.e., they are restricted to be on the unit sphere S^2. Thus the variables can be parameterized into azimuthal angle ϕ and polar angle θ as (X, Y, Z) =$(\sin\theta\cos\phi, \sin\theta\sin\phi, \cos\theta)$.

As the chaoticity parameter κ is varied the classical dynamics ranges from completely regular motion ($\kappa \leq 2.1$) to a mixture of regular and chaotic motion ($2.1 \leq \kappa \leq 4.4$) to fully chaotic motion ($\kappa > 4.4$) [8]. The classical stroboscopic map in polar coordinates for a set of initial conditions with $\kappa = 2.2$ and $\kappa = 3.0$ is given in Fig.2.1a and Fig.2.1b respectively.

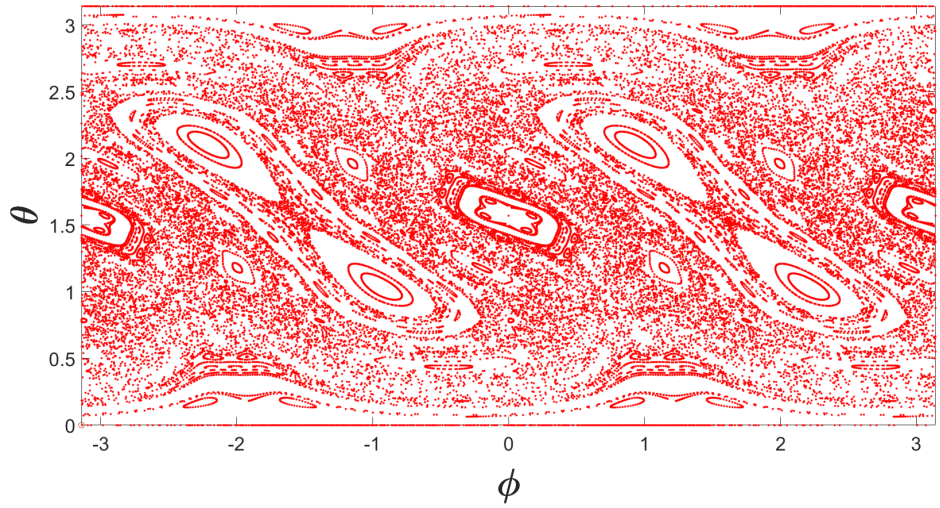

(a)

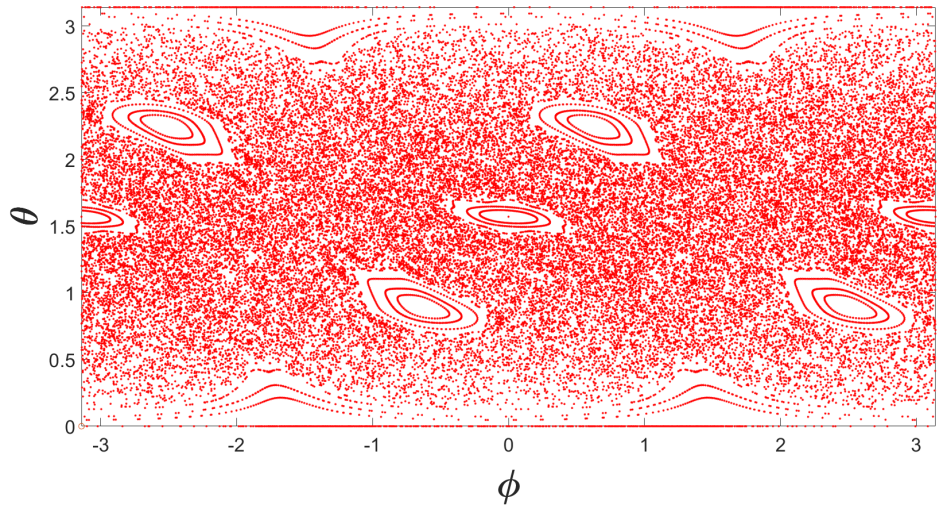

(b)

Figure 2.1: Stroboscopic map showing the classical time evolution over 150 kicks for **(a)**. $\kappa = 2.5$ and **(b)**. $\kappa = 3.0$ for 289 initial points in phase space.

2.2 Spin-coherent state

Spin coherent states (SCS)[46] are minimum uncertainty states in spin systems that satisfy the uncertainty relation

$$\Delta J_i \Delta J_k = \frac{\hbar}{2} |\Delta J_l|, \tag{2.4}$$

where i, k and l are permutations of x, y and z. The uncertainty for these states is distributed symmetrically over the two operators. Given any point (θ, ϕ) in the classical phase space, we construct the corresponding SCS $|j; \theta, \phi\rangle$

$$|j; \theta, \phi\rangle = \exp\left[i\theta(J_x \sin\phi - J_y \cos\phi)\right] |j, j\rangle \,. \tag{2.5}$$

In the $2j$-qubit space, we define our initial states as the SCSs

$$|j; \theta, \phi\rangle = |\theta, \phi\rangle^{\otimes 2j} \,, \tag{2.6}$$

where $|\theta, \phi\rangle$ are points on the Bloch sphere. For larger j values, the SCS becomes highly localized around the point (θ, ϕ) in the phase space. Hence in the classical limit of $j \to \infty$, the SCS approximates the classical angular momentum state located at (θ, ϕ) [4].

Spin-squeezed states, which have an asymmetric distribution of uncertainty, can display entanglement in the corresponding multi-qubit representation[47]. Since we are interested in studying entanglement that arises from the dynamics of the system, we choose SCSs as our initial states, thus ensuring there is no initial entanglement between the qubits.

2.3 Husimi phase space distribution and O_{SCS}

To study quantum-classical correspondence in the quantum kicked top, its Husimi distribution is often compared with the classical phase space distribution [8]. The Husimi distribution has also been used as a visual aid to study dynamical tunneling

in the same model [48, 38]. It is a positive valued quasi-probability distribution given by

$$Q(\theta,\phi) = \frac{2j+1}{4\pi} \langle \theta,\phi| \rho |\theta,\phi\rangle \tag{2.7}$$

which is equal to $\frac{2j+1}{4\pi} |\langle \theta,\phi|\psi\rangle|^2$ for pure states; the overlap of a pure angular momentum state $|\psi\rangle$ and spin coherent state $|j;\theta,\phi\rangle$. We drop the normalization constant of $\frac{2j+1}{4\pi}$ from this expression as j remains fixed. For a given state ρ, the maxima of its Husimi distribution corresponds to the measure O_{SCS}. Here O_{SCS} is the maximum overlap of the given angular momentum state (ρ) with any spin-coherent state on the spherical phase space. In the case of multiple maximum values (but same in magnitude), O_{SCS} corresponds to one maximum value. For example, the Husimi probability distribution of $n-$qubit $|GHZ\rangle$ state has two peaks with 0.5 being its value. Here O_{SCS} will be 0.5 for $n-$qubit $|GHZ\rangle$. If the state has O_{SCS} value as 1, i.e., maximum height of the Husimi probability distribution is unity, then the state is considered to be localised at that (θ,ϕ). If the O_{SCS} value is low then state is localised on the phase space. The relation between O_{SCS} and geometric entanglement has been discussed later the section. The Husimi distributions for points $(\theta,\phi) = (\frac{\pi}{2},0)$ and $(2.25,1.0)$ for $\kappa = 2.5$ and various values of N are given in Fig. 2.2a, 2.2b. We see that the Husimi distribution for $(\frac{\pi}{2},0)$ is more delocalized, which corresponds to a lower O_{SCS} value in Fig. 3.10. On the other hand, the Husimi distribution remains more localized, corresponding to a higher O_{SCS} value.

2.4 Measures of entanglement

Entanglement can be used as a signature of chaos. It has been suggested through many studies that the rate of generation of entanglement is enhanced by the presence of classical chaos. Here we will discuss the three different measures of entanglement, the entanglement of formation (concurrence), von-Neuman entanglement entropy, and geometric entanglement.

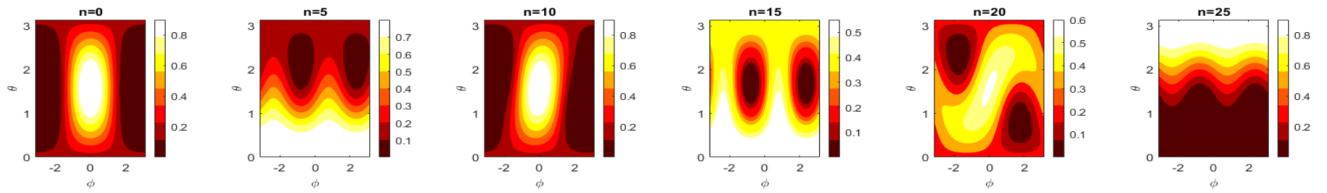

(a)

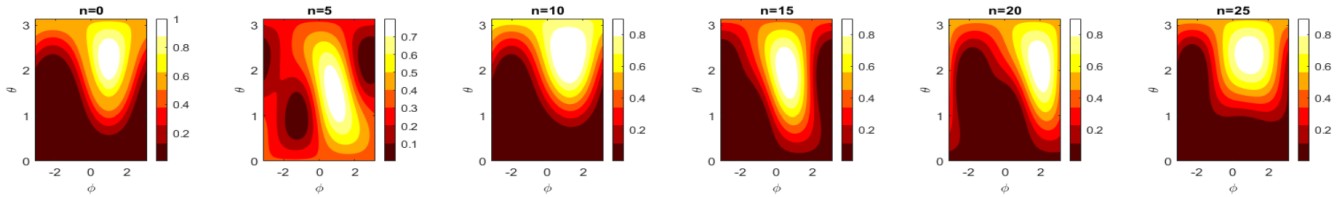

(b)

Figure 2.2: Husimi distribution to visualize delocalization of two different initial states. **(a)** $(\theta, \phi) = (\frac{\pi}{2}, 0)$, **(b)** $(\theta, \phi) = (2.25, 1.0)$ for $\kappa = 2.5$. Here we can see that $(\frac{\pi}{2}, 0)$ is more delocalized.

2.4.1 Concurrence

Entanglement of formation is the most widely used measure of entanglement [49]. For a general state ρ, it is the minimum average von Neumann entropy over all pure-state decomposition of ρ. While this minimum is, in general, challenging to compute efficiently, for two qubits, the concurrence is more popular for quantifying entanglement in two-qubit systems. It is efficient to compute and is a monotonically increasing function of entanglement of formation. Concurrence is computed as follows [50]. For a two-qubit density matrix ρ, first the spin flipped state $\tilde{\rho} = \sigma_y \otimes \sigma_y \rho^* \sigma_y \otimes \sigma_y$ (where σ_y is Pauli matrix and ρ^* is complex conjugate of ρ in the standard basis) is computed. Then concurrence is defined as

$$C = \max(0, \sqrt{\lambda_1} - \sqrt{\lambda_2} - \sqrt{\lambda_3} - \sqrt{\lambda_4}) \tag{2.8}$$

where λ_i are eigenvalues of $\rho\tilde{\rho}$ such that $\lambda_4 \leq \lambda_3 \leq \lambda_2 \leq \lambda_1$ and $0 \leq C \leq 1$. It is 0 for separable states and unity for the Bell states. The relationship between concurrence and chaos has been investigated in previous works [51, 52].

2.4.2 von-Neuman entanglement entropy

Quantum kicked top with spin-j, has a multi-qubit representation in the symmetric subspace of $(2j+1)$ dimensional Hilbert space. A qubit picture of a quantum kicked top can always be represented as a bipartite system. A natural measure of entanglement in bipartite pure states is the von-Neumann entropy of its reduced states [53], S. It is well-defined for pure states. Since at any given time our system is in the pure state, von-Neumann entanglement entropy is a good measure for entanglement in our system. It is defined as

$$S = -\operatorname{Tr}(\rho_{sq} \log \rho_{sq}) = -\sum_{i=1} \lambda_i \log(\lambda_i) \tag{2.9}$$

where λ_i(i=1,2) are eigenvalues of the single qubit density matrix ρ_{sq}. If the qubit is in a pure state, then the single-qubit state is completely known and the entropy is zero.

However, if the qubits are entangled with any other qubit(s), then ρ_{sq} is a statistical mixture of states and the entropy is non-zero. It satisfies the equation $0 \leq S \leq log(2)$.

2.4.3 Geometric entanglement

The extent of entanglement in a pure quantum state can be characterized by its distance to the nearest separable state [54]. This measure of entanglement is commonly known as geometric entanglement, which was first introduced by Shinmoy in 1995 [55]. For a symmetric state $|\psi\rangle$, the geometric entanglement is given by [56]

$$E_G(|\psi\rangle) = 1 - G(\psi)^2 \tag{2.10}$$

where the quantity $G(\psi)$ is the overlap of $|\psi\rangle$ with the closest product state

$$G(\psi) = \max_{|\phi\rangle = |a\rangle|b\rangle|c\rangle \ldots} |\langle\psi|\phi\rangle|. \tag{2.11}$$

Geometric entanglement can be also used to quantify delocalization for symmetric states as discussed in previous section 2.3.

Chapter 3

Quantum simulations of chaos in the deep quantum regime

This chapter is based on Anand, Srivastava, Gangopadhaya and Ghose [39]

Classical chaos is characterized by exponential sensitivity to initial conditions quantified by the Lyapunov exponent, which is a measure of the rate of divergence of neighboring trajectories [57, 58, 59]. A corresponding quantum measure of chaos is challenging to define due to the uncertainty principle and the linearity of quantum evolution. The question of how classical chaos emerges from quantum dynamics remains one of the open fundamental questions in quantum theory [2, 4, 13]. In recent years, the question of quantum-classical correspondence in classically chaotic systems has been explored in the context of quantum information processing. The connection between fundamental quantum phenomena such as entanglement and classical chaos has puzzled physicists for decades and has gained new relevance for quantum computing applications. It has been shown that classical chaos can affect the implementation of quantum computing algorithms [60, 61]. Chaos can also affect the generation of dynamical entanglement, an important resource for quantum computing[33, 62].

Efficient quantum simulations of chaotic models will be a progressive step toward understanding this field. Large-scale, programmable quantum computers could

offer exactly this type of possibility of mapping and simulating complex quantum systems [63]. While such large-scale quantum computers do not yet exist, it is worth exploring the potential for quantum simulations using currently available noisy intermediate-scale quantum (NISQ) computers [44, 64]. One such potential area of NISQ application is the topic of quantum chaos - the study of quantum systems that exhibit chaos in some classical limit. On the experimental side, the quantum control and precision needed to explore quantum chaotic dynamics over a wide range of parameters and long-time scales remain quite challenging. So far, relatively few experiments in limited parameter regimes and for short times have been performed [7, 5, 65, 66, 67].

To understand chaos in the quantum context, it is important to explore signatures of classical chaos in the deep quantum regime, where the standard Bohr correspondence principle cannot be invoked. A textbook model for studying quantum chaos is the quantum kicked top (QKT) [4], which is a finite-dimensional spin system that displays chaotic dynamics in the classical limit. The quantum kicked top has been extensively studied theoretically [33, 34, 6, 36, 37, 35, 52, 68]. Different quantum correlations such as entanglement, discord, and the Mallech Q measure [35, 37, 38] have also been used to study signatures of chaos in quantum dynamics. Among these correlations, quantum entanglement has shown promising results in studying signatures of chaos in the quantum kicked top model (QKT). QKT has been well studied theoretically in semi-classical regions where entanglement has been used to distinguish between regular and chaotic regions of phase space [34, 9, 35, 2, 36, 69]. In recent theoretical studies, the quantum kicked top consisting of just two qubits, belonging to the deep quantum regime, has also been studied in detail [5, 35]. In the deep quantum regime, periodicities and symmetries in the two- and three-qubit QKT model were theoretically studied in [36, 35]. A few experimental studies of the QKT have also been performed [5, 67, 7]. In [7], a 3-qubit model of the QKT was shown to exhibit ergodic dynamics, and a resemblance between entanglement entropy and classical phase space dynamics was noted. Temporal periodicity and symmetries of the 2-qubit QKT were explored using NMR techniques in [5]. These experiments are limited in the number of kicks due to the decoherence times of the physical qubits. Furthermore, in these implementations the chaoticity parameter κ is determined by the strength and duration of interaction

between the qubits, making it difficult to tune. To experimentally study the long-term dynamics and dependence on κ rigorously, one needs to explore longer time scales and a wider range of κ.

The QKT system can be described as a collection of indistinguishable qubits, which makes it attractive to explore in the framework of quantum information processing and NISQ devices. In this chapter, we show that mapping the QKT onto a programmable quantum circuit in a quantum computer allows simulations of the QKT that overcome previous experimental limitations. We construct and demonstrate an exact simulation of the 2-qubit quantum kicked top using a universal set of quantum logic gates. Our quantum circuit-based simulation is programmable and enables flexible initial state preparation and evolution. Using IBM's publicly accessible 5-qubit chip *vigo*, we can prepare initial states and implement the dynamics of the QKT for an arbitrary number of kicks and a wide range of κ. The number of gates required for this simulation is independent of the number of kicks and the value of κ. Therefore, our model does not suffer any systematic loss in fidelity with the increasing number of kicks or κ values. Finally, full quantum state tomography enables us to explore signatures of chaos in 2-qubit entanglement.

The ability to vary κ and the number of kicks allows us to experimentally observe the periodic nature of the dynamics with respect to κ as well as the kick number. Additionally, the temporal periodicity of the QKT can be used to obtain highly accurate time averages of relevant physical quantities. In particular, we explore the time-averaged entanglement for different initial spin coherent states. We find that the contour plot of the time average entanglement shows clear signatures of the classical phase space structures of regular islands in a chaotic sea, even in a deep quantum regime. We also show that the states initialized in chaotic regions of the phase space show intermediate values of average concurrence, whereas the fixed points and the period-4 orbit correspond to the minimum and maximum values respectively. This behavior is related to the degree of delocalization of the states and thus demonstrates a connection between delocalization and entanglement [69]. Our work shows that current quantum computers are useful for flexibly exploring new experimental regimes in quantum chaotic systems. Mapping the system onto a tunable quantum circuit

lets us probe different aspects of the QKT dynamics without the need for building sophisticated customized hardware or being constrained by fixed system parameters. This method combines the ease of numerical simulation with the built-in quantum evolution of a physical system.

The chapter is organized as follows. In section 3.1, we introduce the multi-qubit representation of the quantum kicked top. In section 3.2, our circuit-based approach and the mapping to the IBM *vigo* processor are described. In section 3.3, we discuss the accuracy of the quantum simulations. In section 3.4, we show the periodicity in the concurrence of a two-qubit QKT system. In section 3.5, we discuss entanglement as a signature of chaos for two different κ values. In section 3.6, the experimental results of the IBM *vigo* simulations are discussed. Finally, conclusions, outlook, and the scope of application of our circuit-based approach are discussed in section 3.7

3.1 Floquet operator in qubit space

The QKT Hamiltonian commutes with the total angular momentum operator J^2, $[H, J^2] = 0$. Hence, it can be considered as an $N = 2j$ qubit system [69] confined to the symmetric subspace of $(\mathbb{C}^2)^{\otimes N}$. The spin-$j$ operators are written in terms of the single qubit Pauli rotation operators as:

$$J_\alpha = \frac{1}{2}\sum_{i=1}^{2j}\sigma_{i\alpha}, \quad \alpha \in \{x, y, z\} \tag{3.1}$$

where $\sigma_{i\alpha}$ denotes σ_α acting on the i^{th} qubit. This allows us to rewrite the QKT Hamiltonian in 2j-qubit space:

$$H = \hbar\frac{\kappa}{8j}\left(2j + \sum_{\substack{i,k=1\\ i\neq k}}^{2j}\sigma_{iz}\otimes\sigma_{kz}\right)\sum_{n=-\infty}^{\infty}\delta(t - n\tau) + \hbar\frac{p}{2\tau}\sum_{i=1}^{2j}\sigma_{iy}. \tag{3.2}$$

In particular, the $j = 1$ QKT is described by the 2-qubit Hamiltonian

$$H = \frac{\hbar k}{4}(\mathbb{I} + \sigma_z \otimes \sigma_z)\sum_n \delta(t - n\tau) + \frac{\hbar p}{2\tau}(\sigma_y \otimes \mathbb{I} + \mathbb{I} \otimes \sigma_y) \tag{3.3}$$

and the corresponding single-kick time evolution unitary is

$$U = \exp\left(-i\frac{\kappa}{4}(\mathbb{I} + \sigma_z \otimes \sigma_z)\right)\exp\left(-i\frac{p}{2}(\sigma_y \otimes \mathbb{I} + \mathbb{I} \otimes \sigma_y)\right). \tag{3.4}$$

3.2 Implementation of unitaries with a quantum circuit on IBMQ

Any N-qubit unitary can be decomposed into $2^N(2^N - 1)/2$ single-qubit gates with controls. We follow the prescription in [70] to decompose our 2-qubit Floquet operator as

$$U = U_1 \times U_2 \times U_3 \times U_4 \times U_5 \times U_6, \tag{3.5}$$

where U_i are either single-qubit unitaries or controlled unitaries of the form

$U_i \equiv$ 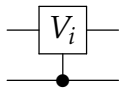 or $U_i \equiv$ 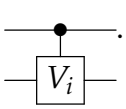 .

In the circuit above, the two wires represent the two qubits, the solid dot represents the control qubit, and the box indicates the single qubit operation V_i on the target qubit. The exact decomposition for a 2-qubit gate in this scheme is

$U =$ 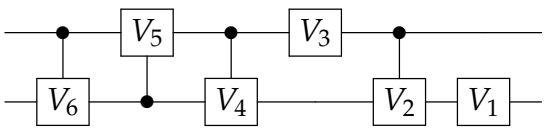 . (3.6)

Implementation of these gates on a quantum computer requires further decomposition into rotations and CNOT gates. Given a 1-qubit unitary W$\in$ SU(2), a controlled gate of the form $(|0\rangle\langle 0| \otimes \mathbb{I} + |1\rangle\langle 1| \otimes W)$ can be decomposed as [71]

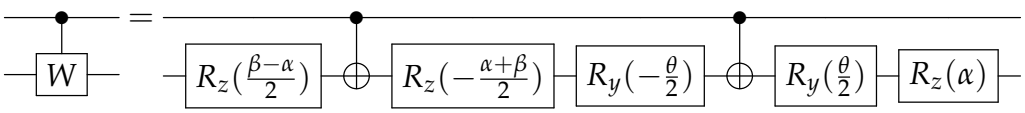

(3.7)

where R_x, R_y and R_z describe rotations on the Bloch sphere and α, β and θ (also known as Euler angles) are such that

$$R_z(\alpha)R_y(\theta)R_z(\beta) = W. \tag{3.8}$$

A general 1-qubit unitary V is of the form $\exp(i\delta) \times W$ where $W \in$ SU(2). A 2-qubit gate of the form $(|0\rangle\langle 0| \otimes \mathbb{I} + |1\rangle\langle 1| \otimes V)$ can be written as

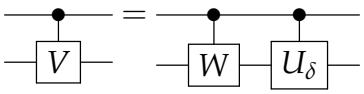

(3.9)

where $U_\delta = \exp(-i\delta) \times \mathbb{I}$. This controlled phase gate can be further simplified by moving the phase over to the other qubit:

$$\begin{aligned}(|0\rangle\langle 0| \otimes \mathbb{I} + |1\rangle\langle 1| \otimes U_\delta) &= (|0\rangle\langle 0| \otimes \mathbb{I} + \exp(i\delta)\,|1\rangle\langle 1| \otimes \mathbb{I}) \\ &= (|0\rangle\langle 0| + \exp(i\delta)\,|1\rangle\langle 1|) \otimes \mathbb{I} \\ &= R_z(\delta) \otimes \mathbb{I}. \end{aligned} \tag{3.10}$$

Here, we ignore a global phase factor of $\exp(i\delta/2)$ in the final step. Finally, we are left with

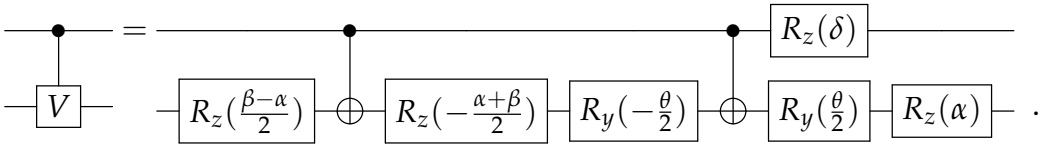

(3.11)

A similar analysis follows when the control and target qubits are exchanged. For two-qubit unitaries of the type $\mathbb{I} \otimes V$ and $V \otimes \mathbb{I}$, the phase factors appearing on V are global and can be ignored. These gates have a similar decomposition as the one in Eq. 3.7 with the CNOT gates replaced by X gates. For example, a unitary of the form $\mathbb{I} \otimes V$ can be decomposed as

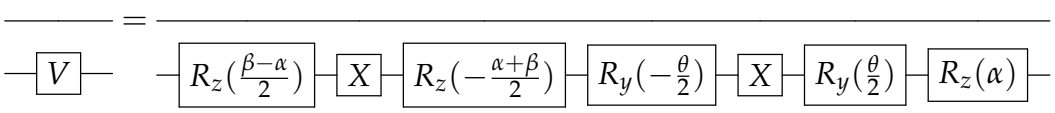

(3.12)

In this scheme, our 2-qubit Floquet operator can be constructed from 46 total gates, with 8 two-qubit CNOT gates and 38 single-qubit rotations. Consecutive rotations have been counted as separate single qubit gates. Depending on the universal gate set for the particular quantum computer, the actual number of gates needed to simulate the Floquet unitary may be reduced.

We implement our quantum circuits on the quantum hardware and simulator back-end of the IBM Quantum Experience [45]. The interfacing with the quantum hardware is done using Qiskit [72]. Qiskit allows us to implement 1-parameter and 3-parameter single-qubit unitary operators of the form

$$U_3(\theta, \phi, \lambda) = \begin{pmatrix} \cos(\theta/2) & -e^{i\lambda}\sin(\theta/2) \\ e^{i\phi}\sin(\theta/2) & e^{i\lambda+i\phi}\cos(\theta/2) \end{pmatrix} \tag{3.13}$$

$$U_1(\lambda) = \begin{pmatrix} 1 & 0 \\ 0 & e^{i\lambda} \end{pmatrix}.$$

We decompose the gates in Eq.(3.6) into a combination of U_1 and U_3 gates. Gates of the form $V \otimes \mathbb{I}$ and $\mathbb{I} \otimes V$ are implemented directly as U_3 gates. For controlled gates, the decomposition given in Eq.(3.9) is used where W$\in$ SU(2) is implemented as a U_3 gate and U_δ is implemented as $U_1(\delta)$. Hence, we obtain the final circuit decomposition for our 2-qubit Floquet operator on IBMQ:

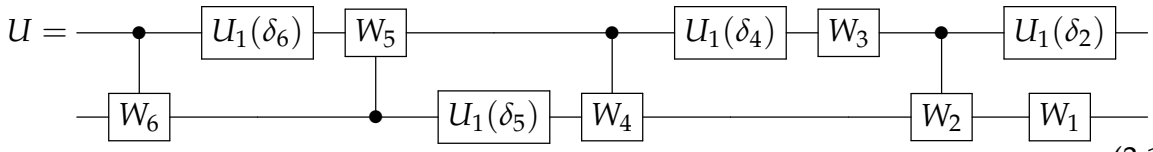

(3.14)

with $W_i = U_3(\theta_i, \phi_i, \lambda_i)$.

An example for the case of $\kappa = \pi$ and $p = \pi/2$ is shown here. The corresponding floquet unitary is decomposed into six single qubit gate and controlled-gate as per Eq. (3.6).

$$V_1 = \frac{1}{\sqrt{2}} \begin{pmatrix} i & 1 \\ -1 & -i \end{pmatrix} \qquad V_2 = \begin{pmatrix} 0 & -1 \\ 1 & 0 \end{pmatrix}$$

$$V_3 = \frac{1}{\sqrt{2}} \begin{pmatrix} 1 & 1 \\ -1 & 1 \end{pmatrix} \qquad V_4 = \begin{pmatrix} 0.688 + 0.288i & -0.688i \\ -0.688i & 0.688 - 0.288i \end{pmatrix}$$

$$V_5 = \begin{pmatrix} i & 0 \\ 0 & -i \end{pmatrix} \qquad V_6 = \begin{pmatrix} 0.688 - 0.288i & -0.688i \\ -0.688i & -0.688 - 0.288i \end{pmatrix}$$

For IBM implementation, V_i's are further decomposed into U_3 and U_1. Parameters for different V_i's for the present case is given below in Table 3.1.

Time evolution after multiple kicks is calculated by applying the Floquet unitary on the initial state repeatedly. This could be achieved by applying the set of gates given in Eq.(3.14) consecutively N times to simulate evolution by N time steps. However, to mitigate the errors which may arise from the increasing number of gates, in our approach, we decompose the effective N-step unitary U^N using the same procedure as mentioned above. This means that the state after any arbitrary number of steps can be obtained by applying the same set of gates given in Eq.(3.14) with appropriate parameters. The advantage of this approach is that the number of gates is fixed and

V_i's	$(\theta_i, \phi_i, \lambda_i, \delta_i)$
V_1	$(\pi/2, \pi/2, \pi/2, -\pi/2)$
V_2	$(\pi, -\pi, \pi, 0)$
V_3	$(\pi/2, 0, 0, 0)$
V_4	(1.5188, 1.8908, -1.2508, -0.3200)
V_5	$0, \pi/2, \pi/2, -\pi/2$
V_6	(1.5188, -3.4616, -0.3200, 0.3200)

Table 3.1: Parameters for U_3 and U_1 corresponding to six V_i for the floquet unitary with $\kappa = \pi$ and $p = \pi/2$

does not grow with the number of kicks. Similarly, time evolution for different values of κ can be implemented by computing the relevant parameters for the set of gates corresponding to the unitary $U^N(\kappa)$. This affords us more fine-grained and flexible control over this parameter compared to other qubit-based realizations where the value of κ is set by tuning the time duration of interactions between the physical qubits.

After applying the appropriate set of gates to the initial states, the final states density matrix is constructed using state-tomography circuits built into Qiskit Ignis[73]. Physical quantities of interest can be calculated from this density matrix.

3.3 Performance of quantum simulations

Starting with various initial points for two different values of κ, we apply the quantum circuit for implementing N kicks on IBM *vigo*. We reconstruct the resulting final state by performing quantum state tomography and use the fidelity of the reconstructed state as a measure of simulation accuracy. For the theoretically predicted state ρ_{th} and the reconstructed state ρ_{vigo}, fidelity is given by $F(\rho_{vigo}, \rho_{\text{th}}) = (\text{tr}(\sqrt{\sqrt{\rho_{\text{th}}}\rho_{vigo}\sqrt{\rho_{\text{th}}}}))^2$. We observe that there is no systematic loss in fidelity with the number of kicks for different initial states and values of κ (Fig.3.1). We compute the average fidelity over different κ values in the range [0.5,6.5] and for different initial states as a function of time. As seen

in Fig.3.2, the average fidelities remain around 0.87.

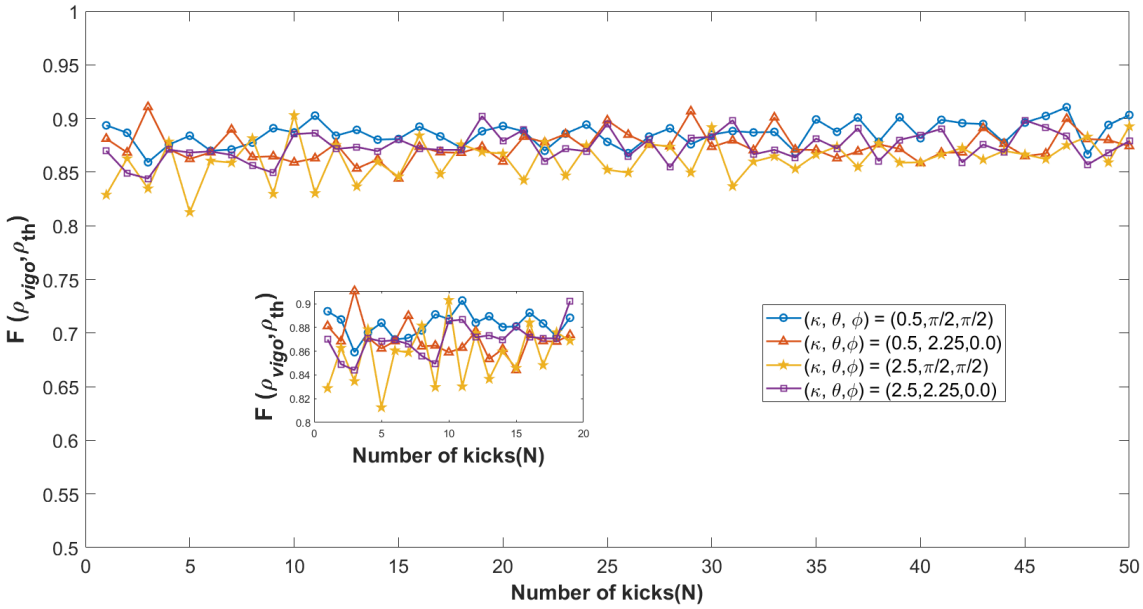

Figure 3.1: Fidelity of the tomographically reconstructed 2-qubit state for different initial states and different κ values on IBM *vigo*. The inset plot shows the small variation in fidelity results due to single qubit and C-NOT gates

Existing experimental implementations of QKT have reported either monotonically decreasing fidelity or a significant drop in fidelity after some particular number of kicks [7, 5]. In this chapter, the non-decreasing trend in fidelity for a higher number of kicks can be attributed to the fixed number of gates for the arbitrary number of kicks. By decomposing the unitary into elementary programmable quantum gates, we effectively remove any constraints on the parameters of the physical system (QKT) that we can implement. In the IBM-Q systems, the error varies only with the number of single qubit physical rotations and CNOT gates [74] acting on each qubit. Since the number of gates in the circuit remains constant irrespective of the value of κ, we observe that the fidelity values do not depend on κ. Average fidelity plots for different initial states as a function of κ are included in Fig. 3.3.

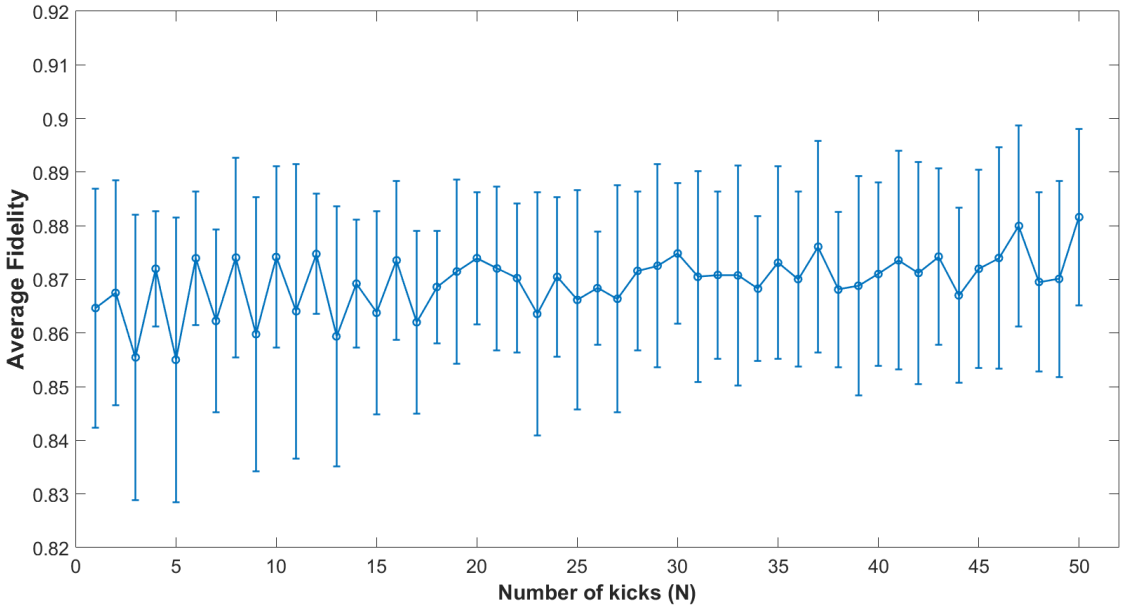

Figure 3.2: Fidelity of the tomographically reconstructed 2-qubit state averaged over initial states with $(\theta, \phi) \in \{(2.25, 0), (\pi/2, \pi/2), (\pi/2, 0)\}$ and $\kappa \in \{0.5, 2.5, 4.5, 6.5\}$ on IBM *vigo*. The error bars indicate the standard deviation.

3.3.1 Errors in IBMQ

We have used IBM Q Experience processors - IBM *vigo* and IBM *quito* - to obtain the experimental results presented in this paper. Both processors have 5 qubits and a Quantum Volume (QV) of 16. These processors were chosen for their low single-qubit and CNOT errors (error values available on the IBM Q experience website). The error in the experimental values also depends on the specific qubits chosen for the computation. For each processor, the computational qubits were chosen to minimize the error. The sources of error can be both statistical fluctuations and systematic errors in the hardware implementation [75]. Relaxation and decoherence of the qubits in a noisy environment are major sources of systematic errors. The CNOT Gate, which involves two-qubit operations is ten times as noisy as the single-qubit rotations. This is because of higher errors introduced by unwanted qubit interactions during the implementation

of multi-qubit operations. There are also read-out errors introduced by the final quantum measurement process. These errors could be theoretically modeled and the experimental data could be filtered to account for them. Quantum error-correcting circuits could also be used to mitigate systematic errors. This could lead to better agreement between theoretical and experimental values of the physical quantities like concurrence. However, we do not investigate error mitigation in this work.

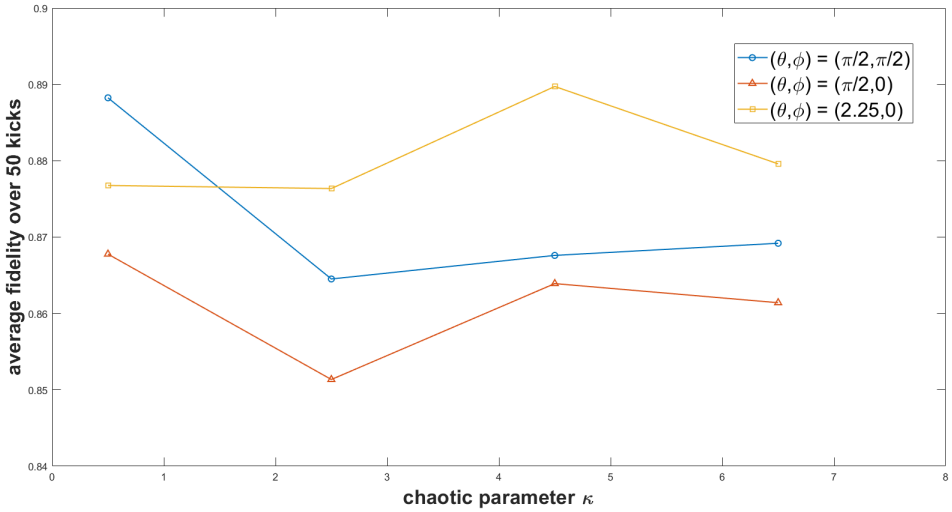

Figure 3.3: Average fidelity for 3 different initial conditions and 4 values of κ. We see that irrespective of the initial points or value of the chaoticity parameter, the average fidelity is within the expected range. We conclude that the initial states or chaoticity parameter values do not affect the average fidelity.

Since IBMQ Experience devices are universal quantum computers, one can implement any unitary transformation using quantum circuits which are composed of basic quantum logic gates (single qubit rotations and the CNOT operation). The 2-qubit quantum kicked top circuit was composed in IBM's Qiskit - a Python-based programming language for the IBM Q Experience. Each circuit was run for 5000 shots to obtain the measurement statistics. State tomography was performed using the tools provided by Qiskit for the reconstruction of the density matrix. The reconstructed

density matrix was used to calculate the relevant physical quantities such as fidelity and concurrence.

3.4 Periodicity of concurrence as function of chaos parameter and number of kicks

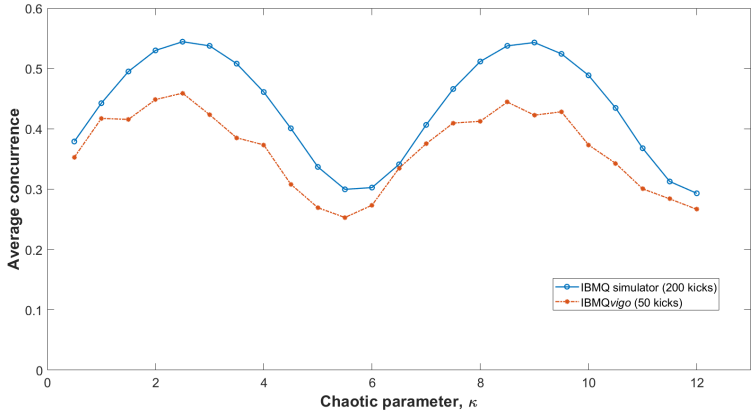

Figure 3.4: Average concurrence plotted against κ show a periodicity of 2π. The initial state was an SCS with $\theta = 2.25$ and $\phi = 2.0$. The average was taken over 200 steps for the simulated plot and over 50 steps on IBM-Vigo.

In this section, we study the periodic nature of concurrence in the quantum kicked top model as a function of both kick strength κ and the number of kicks. We studied this periodic behavior by doing quantum simulations on the IBMQ simulator and reproducing it experimentally on IBM Quantum hardware by using the gate-based approach described in section 3.2. Here, for initial states, we have considered spin coherent states as described in chapter 2. The initial SCS's can be written as a product of a multi-qubit product state and thus exhibits zero entanglement (concurrence).

Initializing our qubits into spin coherent states, we calculate the average concurrence between the qubits for 25 different values of κ ranging from 0 to 12. For a given value of

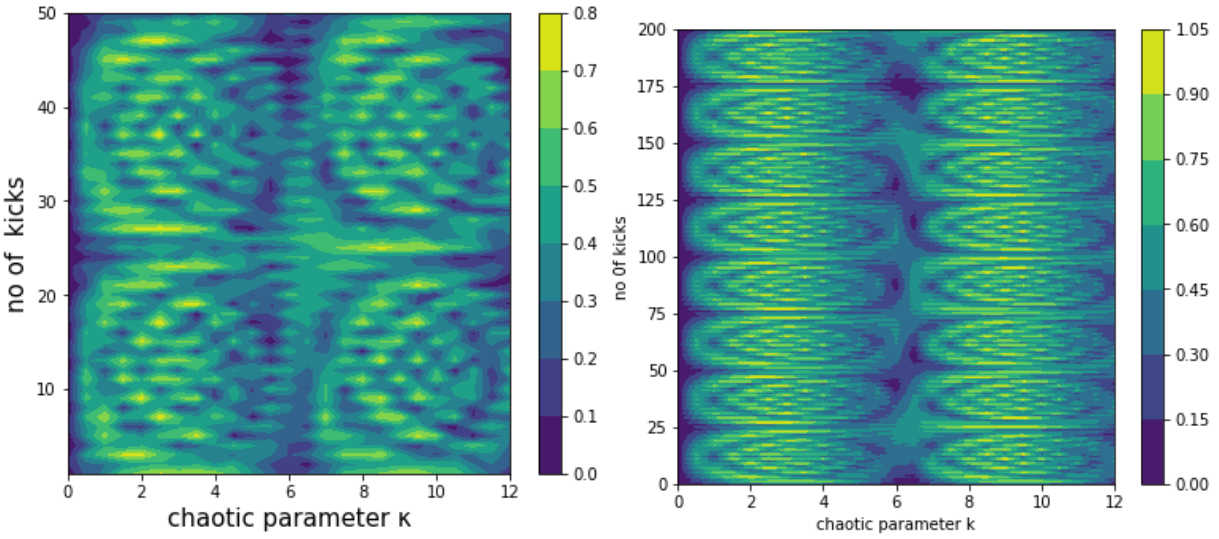

(a) (b)

Figure 3.5: **(a)**. A contour plot of concurrence over 50 kicks and different values of κ on IBMQ-vigo. **(b)**. A contour plot of concurrence over 200 kicks and different values of a kappa on IBMQ simulator

κ, the initial SCS was evolved using the circuit given by Eq.(3.14). The state was evolved upto 200 kicks on the IBMQ simulator and for 50 kicks on IMBQ-Vigo to obtain the final state as $\left|\theta_f, \phi_f\right\rangle = U^n \left|\theta_o, \phi_o\right\rangle$. The number of kicks on real hardware is taken to be less than the simulator to reduce the computational time. For each kick, state tomography is performed on the final state, and then concurrence is calculated using Eq.(2.8) on the reconstructed density matrix. The average value of concurrence, i.e., average over 200 kicks on the simulator and 50 kicks on real hardware is plotted against chaotic parameter κ in Fig.3.4.

A period of κ=2π was observed in both simulators as well as on real hardware. The difference in the value is due to the presence of error in real quantum hardware. To study the periodicity in kicks, a contour plot was made as shown in Fig.3.5a and Fig.3.5b for evolution performed on IBMQ-Vigo and IBMQ simulator, respectively. A period of 25 kicks can be seen in both plots.

To our knowledge, the periodicity of quantum correlations in the 2-qubit QKT model has been explored experimentally in only one previous study by Krithika et.al. In 2018 [5], they only considered four different values κ and up to 8 kicks. Contrary to that, by taking the gate-based approach, we have a much broader range of kicks and chaotic parameter values. In 2018, Bhosale and Santhanam [36] had done a detailed study on the periodic behavior of different quantum correlations such as quantum discord, von-Neumann entropy, concurrence, 3-tangle, and Meyer and Wallach Q measure analytically and by numerical simulations as a function of kick strength κ and several qubits, j. They had shown that for a fixed value of j and a given initial state, the quantum correlations are periodic in κ, with $\kappa = 2j\pi$ being its periodicity. In another work by Ruebeck et al. [35], they had shown exact (quasi-)periodicity in entanglement as a function of the number of kicks, and kick strength was shown. The results that we obtained in our study are in strong agreement with the existing experimental and theoretical results.

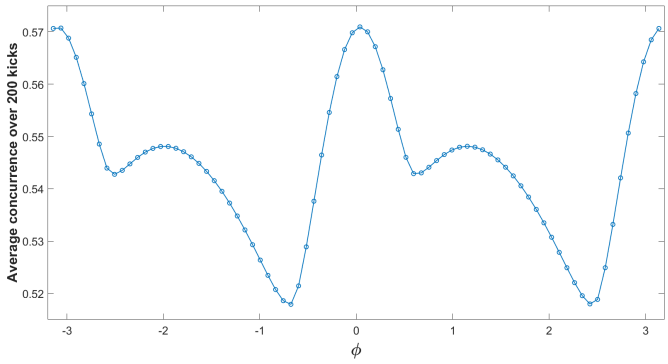

(a)

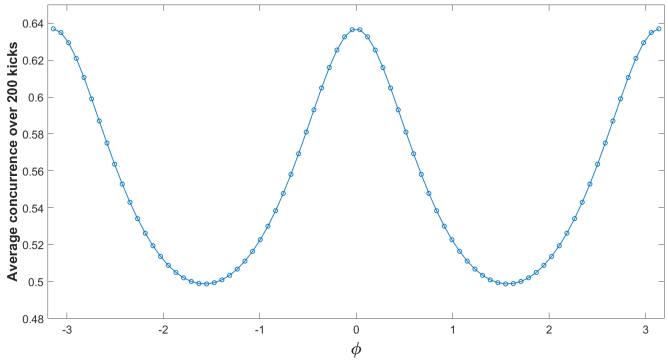

(b)

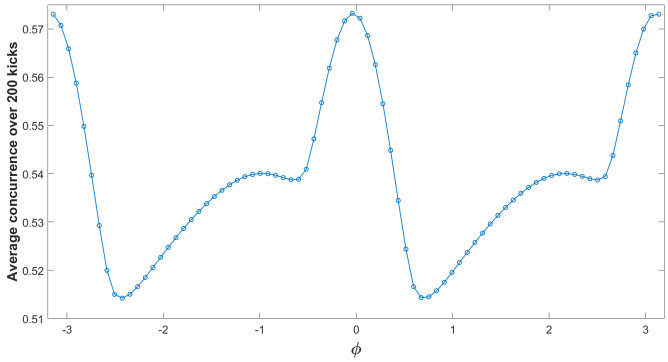

(c)

Figure 3.6: **(a)**.Average concurrence over 200 kicks over 40 divisions in ϕ for $\theta = 0.8$ and k=3.0 **(b)**.ϕ for $\theta = \pi/2$ and k=3.0 **(c)**.ϕ for $\theta = 2.25$ and k=3.0 on IBMQ simulator

3.5 Evolution of entanglement and signatures of chaos

In this section, we analyze the evolution of entanglement and its relationship to mixed chaotic-regular classical phase space. The concurrence is taken as a measure of entanglement for quantum kicked top with j=1. We consider two different values of κ, κ=3.0, and κ=2.5. Different initial states are chosen from the phase space by taking different values of (θ, ϕ) shown in Fig. 2.1a and Fig. 2.1b. These states are spin-coherent states and have zero entanglement and minimum uncertainty value. Each state is evolved for many kicks by using the quantum kicked top circuit model described in 3.3.

3.5.1 Case A. Chaotic parameter $(\kappa) = 3.0$

For κ=3.0, the classical phase space plot is shown in Fig. 2.1b. There are four different regular islands present for this κ value. These regular islands are centered at (θ, ϕ)=(2.25, -2.5),(2.25, 0.63),(0.8,-0.7),(0.8,2.5). To study the effect of these islands on average concurrence, we fix the value of θ as 2.25 and 0.8 as the islands lie on these two lines drawn on the phase space. By fixing the value of θ=0.8, we scan the classical phase space by taking different values of ϕ along these lines. In the range of $-\pi$ to π, we had taken 80 different values of ϕ. Each of these 80 initial points in phase space was evolved in an IBMQ simulator using a QKT circuit, and average concurrence was calculated. The average concurrence vs ϕ is shown in Fig. 3.6a. The same is repeated for $\theta = \pi/2$ and $\theta = 2.25$ given in Fig. 3.6b and 3.6c respectively.

The minimum value of the average concurrence in Fig.3.6a and 3.6c corresponds to the fixed points and Period-2 points in classical phase space dynamics. All four points in the classical phase space mentioned earlier in this section have minimum average concurrence. As we moved out of these points to chaotic seas through regular regions, we saw a rapid rise in the average concurrence. To our surprise, these sudden rises in average concurrence as we came out of islands to the chaotic sea were witnessed in all four islands centered at different points in phase space. These observations led us to do further investigation of these signatures in $\kappa = 3.0$.

Instead of fixing θ to only two values, here we considered the range of θ. We took 9 different values of θ in the range of 0 to π. For each given θ, 17 different values of ϕ were taken in the range of $-\pi$ to π. Average concurrence was calculated for all 153 points after evolving for 200 kicks. Different curves corresponding to different values of θ were plotted against ϕ as shown in Fig. 3.7a and Fig. 3.7b. The curves passing through the islands i.e. θ=0.8(yellow) and θ=2.4 (red) show different curvature in the region where we have the island in the classical phase plot, as shown in Fig. 3.7a and Fig. 3.7b respectively.

An initial SCS centered on the regular island exhibits a slow increase in the average concurrence and undergoes quasi-periodic dynamics, while an SCS in the chaotic regime shows a faster initial increase in concurrence and a more irregular evolution. This effect can be seen in the plot. This difference is due to the structure of the classical phase plot. Here, islands on the classical phase space can be identified using a concurrence plot. As we move out of the regular islands, the sudden increase in average entanglement gives us a signature of chaos in quantum dynamics. In [33, 34, 6], the detailed theoretical study showed entanglement as a signature of chaos in quantum dynamics for large values of j or in the semi-classical region. It is interesting to note that our entire work is done in the deep quantum regime, but we can still see entanglement as a clear signature of chaos in QKT dynamics. In our simulated results, we also show that for any given value of θ, the maximum value of average concurrence is obtained for $\phi = m\pi$ where m is an integer. This is because these initial points belong to the period four orbits as discussed in [35] .

3.5.2 Case B. Chaotic parameter $(\kappa) = 2.5$

In the classical phase space for κ=2.5, the regular regions are not as localized as in $\kappa = 3.0$. The regular regions are spread out in phase space, and the regular and chaotic seas are not well separated. Here, we take 9 divisions in θ in the range of 0 to π. This range of θ covers all the four regular regions in phase space of classical dynamics for $\kappa = 2.5$ (Fig 2.1a). For a given value of θ, we further consider 17 different values of ϕ in the range of $-\pi$ to π. Each combination of (θ, ϕ) is taken as an initial spin coherent state and

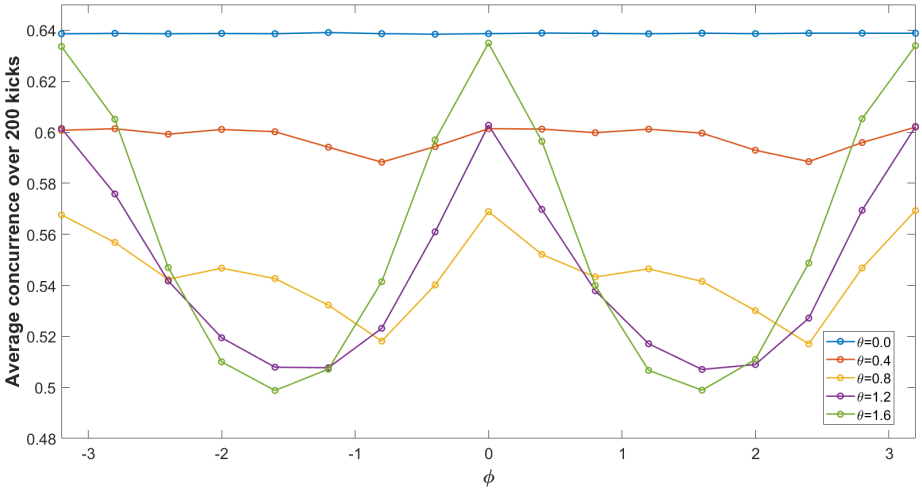

(a)

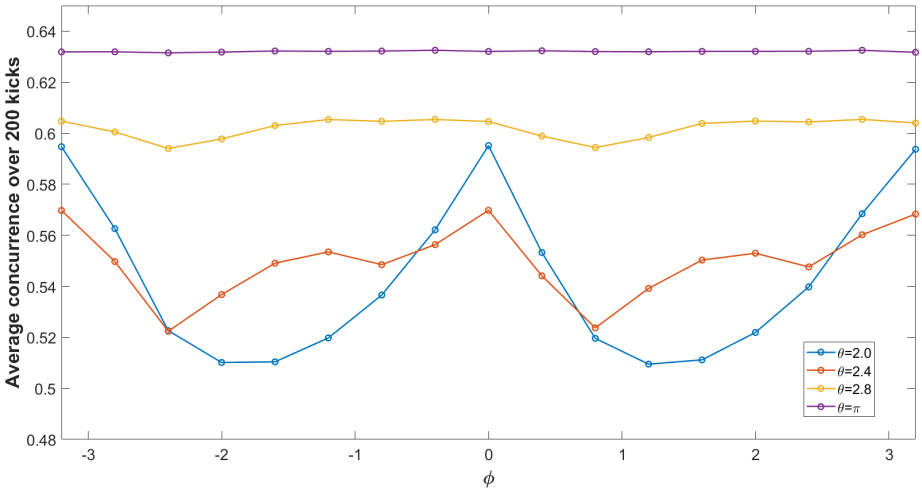

(b)

Figure 3.7: Average concurrence over 200 kicks and 17 divisions in ϕ for (**a**) $\theta = 0.0$ to 1.6 and $\kappa = 3.0$ (**b**) for $\theta = 2.0$ to π and $\kappa = 3.0$ on IBMQ simulator

evolved quantum mechanically using a QKT circuit for 200 kicks. Average concurrence is calculated for 17 different sets of initial points for fixed θ and plotted against ϕ. For all 9 values of θ the results are illustrated in Fig 3.8a and Fig. 3.8b.

Here we do not see any irregular nature in the curve that passes through the islands, unlike the previous case. This is because for $\kappa = 2.5$, the regular regions are not completely isolated, and there is no sudden change in the classical dynamics as we move out of the fixed points. However, the global minimum value for the average concurrence (i.e minimum value for the green and blue curve in Fig 3.8a and Fig. 3.8b respectively) corresponds to the center of the regular regions.

3.6 Relationship between entanglement and delocalization

The periodicity in concurrence, combined with the ability to implement a high number of kicks, can be exploited to generate detailed average concurrence plots. By averaging over multiple periods of concurrence in the number of kicks, we can reduce the error in the value of average concurrence. This allows more detailed observations of signatures of chaos in entanglement dynamics.

A contour plot of time-averaged concurrence as a function of θ and ϕ for $\kappa = 2.5$ reflects the structures of the stroboscopic classical map as shown in Fig.3.9. Furthermore, our plots have enough resolution to observe that the chaotic regions of the classical phase space show intermediate concurrence values. The four prominently visible islands of low concurrence correspond to fixed points of the classical dynamics. These islands are distinguishable on the hardware plot and the left-right symmetry is maintained as shown in Fig.3.9c. Points $(J_x/j, J_y/j, J_z/j) = (1,0,0), (0,0,-1), (-1,0,0)$ and $(0,0,1)$, which constitute a period-4 orbit present in the classical dynamics of the system, show the highest values of average concurrence [35, 37, 7, 5]. The contour plots of average concurrence for various values of κ obtained on the IBMQ simulator are included in Section 3.6.1.

We note the correspondence between the average concurrence and the degree of delocalization of various initial states after evolution using the Floquet unitary. This

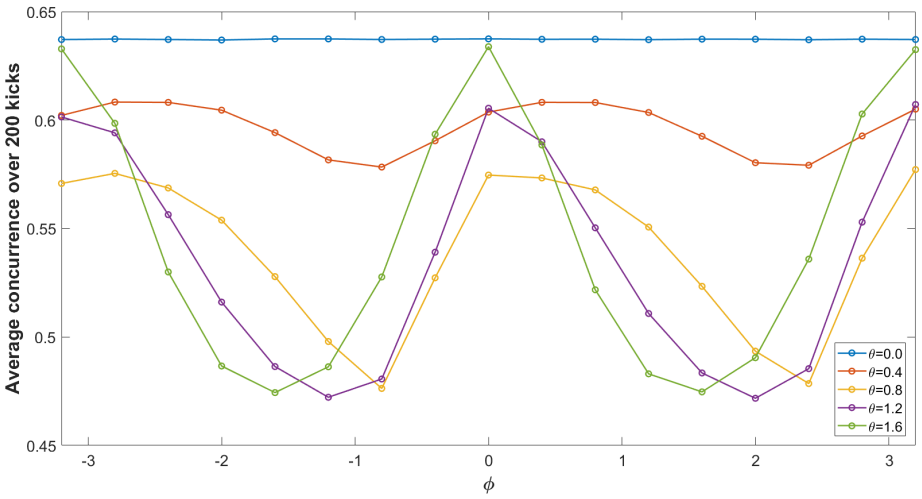

(a)

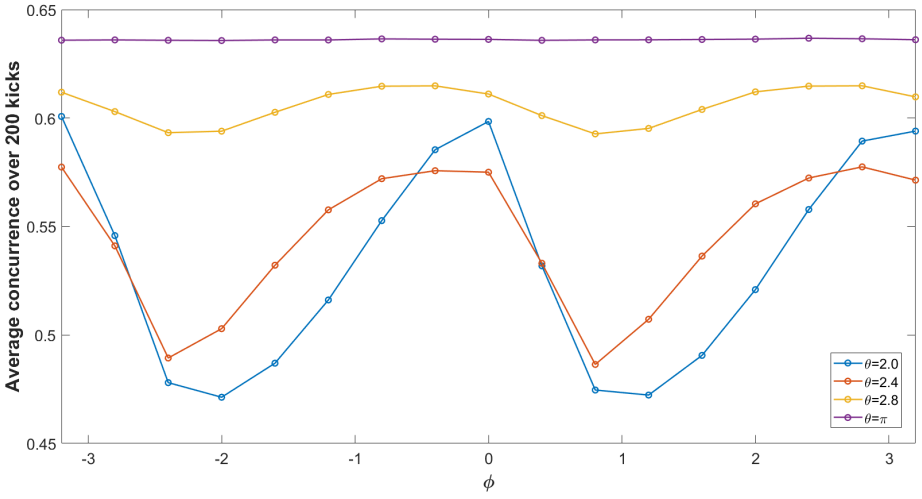

(b)

Figure 3.8: Average concurrence over 200 kicks over 17 divisions in ϕ for (**a**) $\theta = 0.0$ to 1.6 and $\kappa = 2.5$ (**b**) for $\theta = 2.0$ to 3.6 and $\kappa = 2.5$ on IBMQ simulator

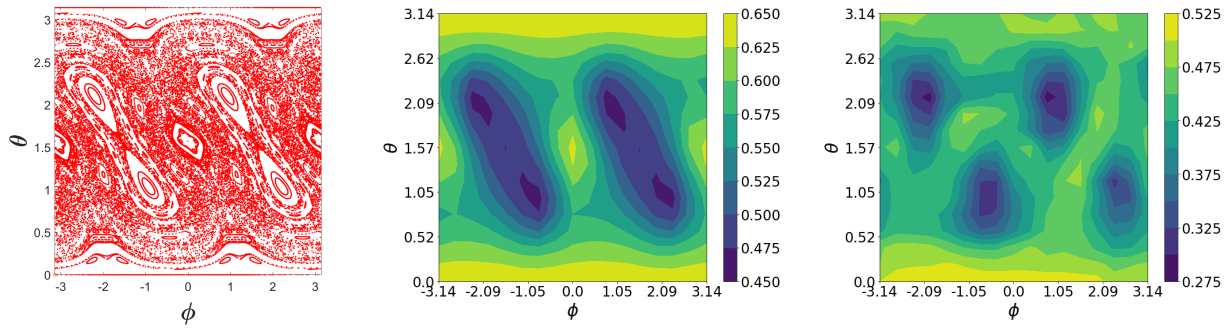

(a) (b) (c)

Figure 3.9: Comparison between classical phase space and contour plot of average concurrence. (a) Stroboscopic classical map, (b) average concurrence over 200 kicks on IBMQ simulator and (c) average concurrence over 50 kicks on IBMQ *vigo* for 289 initial points and $\kappa = 2.5$.

degree of delocalization [69] can be quantified by calculating the maximum overlap with respect to the set of minimum uncertainty spin coherent states.

$$O_{\mathrm{SCS}}(|\psi(t)\rangle) = \max_{\mathrm{SCS}} |\langle \mathrm{SCS} \mid \psi(t)\rangle|. \tag{3.15}$$

Large values of O_{SCS} correspond to more localized states, as they indicate high overlap with spin coherent states. Delocalized states show low O_{SCS} values. The values of O_{SCS} for two different initial states, one in the high concurrence region and one in the low concurrence region, are plotted against the number of steps in Fig.3.10, and show the connection between entanglement and delocalization. The corresponding Husimi distributions for these points are shown in Section 2.3 (Fig.2.2).

This approach of quantifying delocalization is equivalent to the definition of geometric entanglement given in [56] (see section 2.4.3). Since all the spin coherent states are separable, and every symmetric separable state of this Hilbert space is a spin coherent state, for our case the quantity $G(\psi)$ is exactly equal to the previously defined $O_{SCS}(|\psi\rangle)$. Hence, this definition implies that highly delocalized states have higher geometric entanglement and more localized states have lower geometric entanglement.

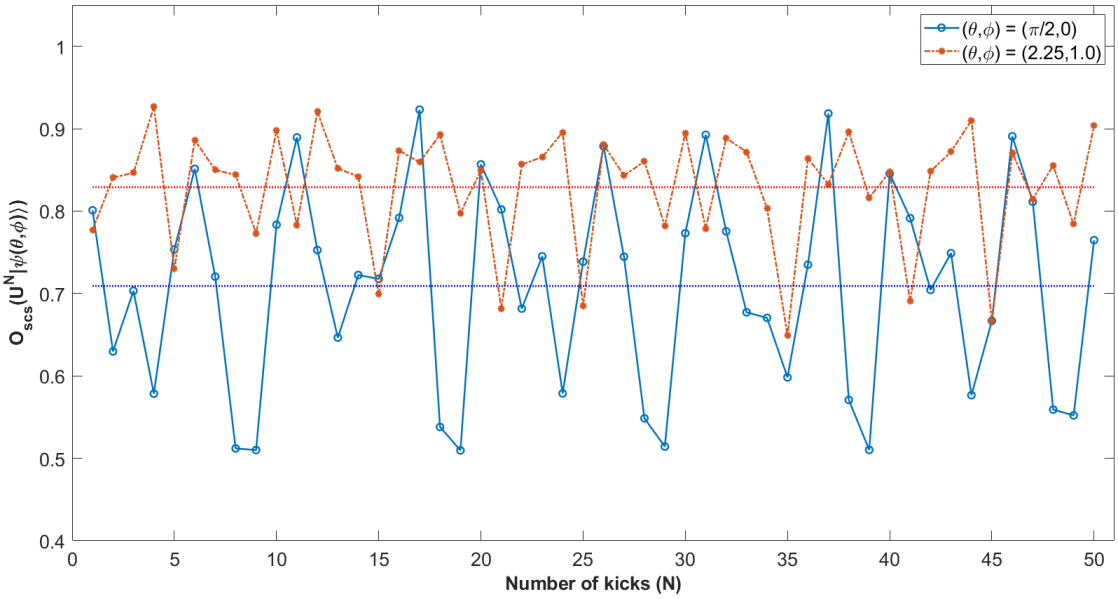

Figure 3.10: Evolution of O_{SCS} values for two different initial states for 50 kicks on IBMQ *quito*. The evolution of initial state leading to higher concurrence ($(\theta, \phi) = (\pi/2, 0)$) is more delocalized, i.e., has lower average O_{SCS} than that corresponding to lower concurrence ($(\theta, \phi) = (2.25, 1)$). The horizontal dotted lines represent the average O_{SCS} values for the two cases.

This behavior, in the case of the 2-qubit QKT, agrees with the trend in concurrence. This observation of the connection between entanglement and delocalization in the deep quantum regime confirms previous theoretical predictions [69, 76].

3.6.1 Average concurrence contour plots for different values of κ

Here, we show the correspondence between the classical phase space and the average concurrence contour plots for different values of κ in the range 0 to π. For low values of the chaoticity parameter (say, $\kappa = 1$), the classical phase space is dominated by regular regions.

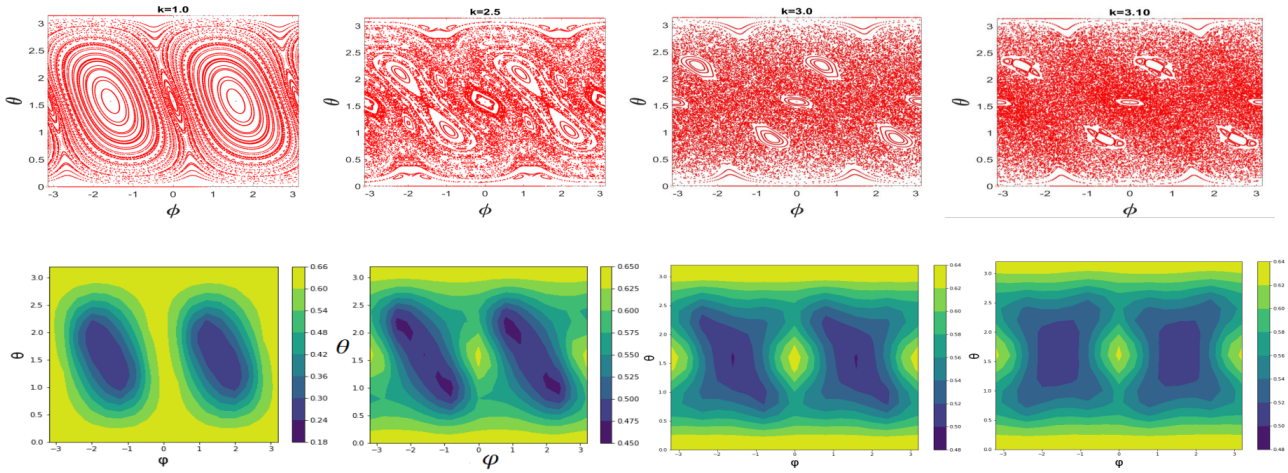

Figure 3.11: Classical phase space and the corresponding average concurrence contour plots for $\kappa = 1.0, 2.5, 3.0$ and 3.10. The contour plots have been obtained by averaging over 200 kicks on the simulator backend of IBMQ.

In this case, the corresponding contour plot of concurrence reflects this regular structure of the phase space which is consistent with the behavior as mentioned in the results in Section 3.6, i.e., the lowest average concurrence values correspond to the fixed points, intermediate values to chaotic regions and highest values appear for the points of period-4 orbits. For higher values of κ, the features in the quantum dynamics become too localized to be exactly resolvable by the contour plots of 2-qubit average concurrence. However, we note that the contour plots for $\kappa = 3.0$ still accurately reflect the behavior of the phase space regions as stated in results in Section 3.6. We have considered the range $\kappa = (0, \pi)$ as for the 2-qubit case the concurrence behavior is symmetric about $k = \pi$ (Fig. 3.4) with 2π being the periodicity.

3.7 Summary

In this chapter, we have proposed a quantum circuit-based approach to simulate and explore quantum chaos and demonstrated its advantages over existing methods. The proposed method can be applied in general to any periodically driven

finite-dimensional quantum system. In our study, IBM's 5-qubit open-access quantum chip (*vigo*) was used as the experimental platform to implement the proposed approach for the 2-qubit quantum kicked top (QKT). The Hamiltonian of the QKT can be exactly expressed in terms of qubits since it is a finite-dimensional quantum system. Therefore, its evolution operator can be decomposed into quantum gates. Traditionally, experimental studies of quantum chaos have applied the same set of operations n times to explore time evolution. Here, we decomposed the unitary evolution operator for n kicks, U^n, into elementary quantum gates. This results in a fixed number of operations implementing the QKT evolution for any number of kicks. This hybrid combination of classical processing and quantum computing opens up the ability to perform high-fidelity experimental studies of quantum chaos in new parameter regimes. Previous experiments also showed that chaos affects the efficiency of experiments. The fidelity drops rapidly if the initial state lies in classically chaotic regions, compared to regular regions. However in our approach, it can been seen that location of the initial state on classical phase space, i.e., chaotic or regular does not affect the implementation of the gates. It can been seen from Fig. 3.2 that average fidelity remains almost same for chaotic and regular initial points. This shows that our method of implementing the chaotic Hamiltonian is insusceptible from the intrinsic chaos and noise in the system is only due to the systems' architecture.

Our results demonstrate the advantages of circuit-based NISQ devices for exploring fundamental questions in quantum information and quantum chaos despite their noise and scale limitations. Previous studies [60, 61] have noted that chaos could influence the efficient and stable operation of quantum computers. In [77], it was shown that chaos affects the balance between the disorder that maintains the stability of qubits and nonlinear resonator couplings that are used to manipulate interactions. This plays an integral role in future transmon device engineering. The gate-based circuit model of QKT can be used as an efficient tool for studying these fundamentals questions in the field of quantum information and quantum chaos where these effects are prominent.

Since the value of the chaoticity parameter, κ only determines the parameters of unitary rotations in the quantum circuit, and since the single qubit rotation errors are independent of the parameters, we were able to experimentally study chaotic

dynamics over a wider range of κ and kick number than were previously accessible to experimental studies. By taking advantage of the high fidelity obtained for both a large number of kicks and arbitrary κ values, we experimentally demonstrated the periodicity of entanglement with time and κ with high accuracy. We have shown that average concurrence can be taken as a clear signature of chaos in quantum kicked-top motion. It can be used to identify the regular or chaotic regions of the phase space. Our studies also clearly showed the signature of chaos in the contour plot of average 2-qubit concurrence despite being in the deep quantum regime. The time average concurrence plot contains all the structure of the mixed-classical kicked-top phase space along with different features with great accuracy. It confirms that there is a strong correspondence between classical and quantum chaotic dynamics. Our studies of dynamics in the deep quantum regime shed new light on the quantum-classical correspondence by showing that clear signatures of classical chaos can be identified far away from the semi-classical regime.

For higher values of j, the approach implemented in the present study to decompose an arbitrary unitary into an elementary quantum gate will require exponentially more classical operations. The number of gates also grows double exponentially as we increase the number of qubits. This will increase the computational cost and introduce more noise while realizing QKT using several qubits. However, many dynamical properties like bifurcation, and period doubling can be studied more explicitly in the QKT when we approach the semi-classical regime [8]. Therefore, it is essential to develop an efficient decomposition of the unitaries to study these physical phenomena in detail. Multiple symmetries in the QKT's floquet operator might allow for a more efficient decomposition technique. Our findings show that despite the noise and scale constraints, circuit-based NISQ devices offer advantages for studying fundamental issues in quantum information and quantum chaos.

We reported the first observation of the correspondence between average entanglement and delocalization in the 2-qubit QKT. However, it should be noted that as we go closer to $\kappa = j\pi$, the quantum-classical correspondence vanishes. We study this phenomenon in the next chapter in detail, showing the breaking of Bohr's correspondence principle for a finite spin and special κ values.

Chapter 4

Quantum recurrence in the kicked top model

This chapter is based on ongoing project with Jack Davis and Shohini Ghose

The quantum-classical correspondence principle generally states that the dynamics of a quantum mechanical system should reduce to some form of classical dynamics in a given appropriate limit [1]. Concrete manifestations of this idea include Bohr's correspondence principle [78], Ehrenfest's theorem [11], and the Liouville correspondence [79, 80]. Such a transition, however, is not always straightforward. It is in general a difficult problem to determine exactly how far along the classical limit a system must be in order for the classical structure to emerge, if at all. Much effort has been put into this question for systems that exhibit classical chaos, where oftentimes a relatively large quantum number must be present to establish a faithful correspondence [8, 81].

Bohr's correspondence principle essentially states that a system constituting large quantum numbers shows classical properties. A natural question that arises in this context is whether this principle always holds for large quantum numbers? In this chapter, our main results contribute to this discussion by describing several families of quantum spin dynamics, each parameterized by the dimension, that do not behave

like the analogous classical dynamics for any finite spin quantum number. We study Bohr's quantum-classical correspondence in the quantum kicked top model [4], which is chaotic in the classical limit. It is a finite-size spin-j system of $(2j+1)$ dimensions. Since it does not suffer from truncation errors, it is a standard model for studying chaos and its quantum signatures. QKT is a periodically driven system, whose global phase space dynamics transits from regular to fully chaotic as the kick strength varies. Previous work on the muti-qubit representation of QKT [33, 34] has shown that classically chaotic points on a phase space have a higher rate of entanglement generation than classically regular points. There are few experimental [7, 39, 5, 67, 82] studies on the small values of j that also show correspondence between classical and quantum phase space dynamics and suggest that entanglement can be used as a signature of quantum chaos. The quantum-classical correspondence becomes more and more distinct as we increase the quantum number j, as the effective $\hbar$ decreases.

The works of Lombardi and Matzkin [9] explicitly demonstrate that the evolution of states with initial centroids within a classically regular region can generate entanglement just as efficiently as those in classically chaotic regions . Using the quantum kicked top model for j=10, they have questioned the correspondence principle by showing that entanglement generation in this model depends on the nature of individual points in classical phase space rather than global behavior. Another observation mentioned in the paper is about the size of the system and how it relates to the classical dynamics and semi-classical regime. In a paper by Kumari and Ghose [8], the authors have analyzed classical periodic orbits and how the stability of these points and bifurcations affect the correspondence principle, showing that $Period-n$ points break the correspondence principle at the onset of chaos. They have prescribed criteria for calculating the quantum number for which one can invoke the correspondence principle for the initial states localized on these periodic points. Furthermore, in a work by Ruebeck et al., [35], $j=1$ QKT was studied, and the author shows that the correspondence principle cannot be invoked in this regime. Even though there was a strong correlation between the classical dynamics and time-averaged entanglement between two qubits, this correlation is not directly related to classical chaos. In another work by Bhosle and Santhanam [36], they showed the temporal periodicity for $j=1$,

and κ equal to a rational multiple of π and conjectured that for $j > 1$, QKT only displays periodic behavior in kick strength (κ).

In all the earlier works, the breaking of the correspondence principle was either related to system size or properties of initial classical points. In our work, which is the focus of this chapter, we show a different way through which Bohr's correspondence principle is violated. The breakdown of the quantum-classical correspondence is observed in the system irrespective of its size or the centroid of the initial state on the phase space. For specific values of the chaoticity parameter (κ) as a function of j, the entire quantum dynamics gets repeated after a certain number of kicks. This temporal periodicity is different for integer and half-integer systems, but it is not large enough. Therefore, it prohibits the system from exploring all possible dynamics contrary to the chaoticity parameter values. Our primary tool is the Pauli group of quantum information and the symmetric multi-qubit realization of the SU(2) representation that houses the kicked top. As a consequence of this temporal periodicity, the quantum dynamics are entirely different for those parameters, which were not observed primarily. Recent work [83] has proposed the so-called pseudo-classical dynamical explanation of the dynamics when the chaoticity is slightly perturbed away from the recurrence values, whereas here we focus on (a subset of) the exact values. We also calculate the stability of the periodic points in the neighborhood of these particular κ values and quantify it using von-Neumann entropy. We show that this temporal periodicity is highly stable in the neighborhood of this κ value even for a large number of kicks. We also provide analytic proofs for the periodicity of quantum correlations for all values of j. Our results suggest that for specific values of κ, the system never behaves classically, irrespective of its size. In addition to this observation being an interesting advancement in probing the correspondence principle in the context of chaotic systems, it also may be seen as a (partial) kicked-top manifestation of the *quantum resonance* phenomenon found in the quantum kicked rotor – another important and experimentally feasible model used in the field [84, 85, 86].

In the next section, we provide a short proof of the chaoticity periodicity. This is to

both re-enforce previous studies and establish the information-theoretic framework for the temporal studies. In section 4.2, we analytically prove the temporal periodicity for different values of κ as an integer multiple of $j\pi$ and provide the numerical simulations for the case of half-integer multiples of $j\pi$. In section 4.3, we study the stability of these special values using the von-Neuman entropy and showed that these special values are highly stable to the perturbation for a large number of kicks. In section 4.4, we discuss the outlook and summary of this work.

4.1 Periodicity in quantum correlations

Here is a brief section on the periodicity found in the chaoticity parameter κ. We include it to reproduce previous results using the technique used in subsequent sections. Consider the set of kicked top unitaries parameterized by κ, $\{U_\kappa\}_{\kappa\in\mathbb{R}}$. It is clear that a shift in twist strength $\kappa \mapsto \kappa + 4\pi j$ leaves the unitary invariant: $U_{\kappa+4\pi j} = U_\kappa$. However, from a correlations perspective in the symmetric multi-qubit picture, it was argued in Ref. [36] that the entanglement generated between the virtual qubits is periodic in the chaoticity parameter with period $\Delta\kappa = 2\pi j$. That is to say,

$$U_{\kappa+2\pi j} \overset{\text{LO}}{\Longleftrightarrow} U_\kappa, \tag{4.1}$$

where LO refers to (symmetric) local operations over the global Hilbert space of the qubits. Furthermore, the range of any associated entanglement monotone is equal to the values it takes over evolutions parameterized only by the interval $\kappa \in [0, \pi j]$:

$$U_\kappa \overset{\text{LO}}{\Longleftrightarrow} U_{\tilde{\kappa}}, \qquad \tilde{\kappa} \in [0, \pi j]. \tag{4.2}$$

Presented here is a simpler and more direct proof of these facts, valid for arbitrary spin. As pointed out in [36], there is a recurrent relationship between unitaries separated by an amount $\kappa = 2\pi j$:

$$U_{\kappa+2\pi j} = e^{-i\frac{(\kappa+2\pi j)}{2j}J_z^2} e^{-ipJ_y} = e^{-i\pi J_z^2} U_\kappa.$$

The unitary $e^{-i\pi J_z^2}$ characterizes the difference between the actions of U_k and $U_{k+2\pi j}$ on the Hilbert space. We will show that this operator acts as a symmetric local unitary in the qubit picture, and so does not modify any correlations between the qubits.

Before doing so, we would like to make a brief clarifying comment regarding the unitarity of spin operations. When considering a spin-j system as a permutation-invariant collection of $n = 2j$ qubits, the natural mathematical structure underpinning this is the tensor product representation of the qubit spin observables,

$$J_i := \sum_{k=1}^{n} \frac{\sigma_i^{(k)}}{2}, \qquad \sigma_i^{(k)} = \mathbb{I} \otimes \cdots \otimes \underbrace{\sigma_i}_{k\text{-th tensor factor}} \otimes \cdots \otimes \mathbb{I}. \tag{4.3}$$

where σ_i are Pauli operators. The set of operators $\{J_i\}$ as defined in Eq. (4.3) realize the commutation relations of the $\mathfrak{su}(2)$ algebra, $[J_i, J_j] = i\epsilon_{ijk}J_k$, and form an irreducible representation when restricted to the symmetric subspace [87]. The operators $\{J_i\}$ are still observables over the full Hilbert space $(\mathbb{C}^2)^{\otimes n}$ with well-defined global unitaries as their exponentiations. In this setting, the full multi-qubit Hilbert space is introduced first, then a spin-j system is found to be a closed Clebsch-Gordan subspace thereof. If, however, in the opposite direction, one were to begin with an abstract spin-j system $\{\tilde{J}_i\}$ and isometrically embed it into a larger Hilbert space, then its action on the orthogonal complement would be arbitrary. The extended/lifted operators in principle do not even have to be globally Hermitian nor their exponentials unitary; as in [36], for example, implicitly lifted $e^{-i\theta\tilde{J}_z}$ to a singular operator that annihilates the remaining $2^n - (2j+1)$ dimensions. While this approach leads to the correct conclusions, here we avoid the associated ambiguities by sticking to the perspective of Eq. (4.3) throughout.

With the above in mind, and denoting $Z_k := \sigma_z^{(k)}$, consider the operator $e^{-i\pi J_z^2}$ in the qubit picture:

$$\begin{aligned} e^{-i\pi J_z^2} &= \exp\Big[-i\frac{\pi}{4}(Z_1 + \cdots + Z_N)^2\Big] \\ &= \exp\Big[-i\frac{\pi}{4}\sum_{\vec{k}}\binom{2}{\vec{k}} Z_1^{k_1}\cdots Z_N^{k_N}\Big] \\ &= \prod_{\vec{k}} \exp\Big[-i\frac{\pi}{4}\binom{2}{\vec{k}} Z_1^{k_1}\cdots Z_N^{k_N}\Big], \end{aligned} \tag{4.4}$$

where $\vec{k} = (k_1, ..., k_N)$ is a multi-index of positive integers that sums to 2, and $\binom{2}{\vec{k}}$ is a multinomial coefficient. Separate the multi-indices into those with a single $k_i = 2$ and those that don't; the former will happen n times, and the associated Pauli operator squares to the identity:

$$e^{-i\pi J_z^2} = \exp\left[-i\frac{\pi}{4}I\right]^n \prod_{\vec{k}\neq 2} \exp\left[-i\frac{\pi}{4}\binom{2}{\vec{k}} Z_1^{k_1}\cdots Z_N^{k_N}\right]. \tag{4.5}$$

The remaining indices each have exactly two different slots equal to 1 and so the multinomial coefficient is always 2. The exponentials consequently reduce to

$$\begin{aligned} e^{-i\pi J_z^2} = \quad & e^{-i\frac{n\pi}{4}} \prod_{\vec{k}\neq 2} \left(I^{\otimes n}\cos\frac{\pi}{2} - iZ_1^{k_1}\cdots Z_n^{k_n}\sin\frac{\pi}{2}\right) \\ = & e^{-i\frac{n\pi}{4}} \prod_{\vec{k}\neq 2} \left(-iZ_1^{k_1}\cdots Z_n^{k_n}\right). \end{aligned} \tag{4.6}$$

It is already clear from Eq. (4.6) that $e^{-i\pi J_z^2}$ is a local unitary for an arbitrary spin and so does not affect any correlations between the qubits.

To find a more compact form of Eq. (4.6) and verify that it is furthermore a symmetric local unitary, first factor out the $(-i)$ by noting that the total number of indices $\vec{k}$ is given by $\binom{2+N-1}{N-1} = \frac{N^2+N}{2}$ and so the number of those without a 2 somewhere is $\frac{N^2-N}{2}$. In the remaining product, the composite operator in each fixed tensor factor will consist of exactly $N-1$ Pauli Z operators and $\frac{N^2-N}{2} - (N-1) = \frac{1}{2}(N-2)(N-1)$ identity operators [1]. Altogether this leads to

$$e^{-i\pi J_z^2} = (-1)^{j^2} Z_1^{N-1}\cdots Z_N^{N-1}, \tag{4.7}$$

which is symmetric. This breaks into three cases of spin

$$e^{-i\pi J_z^2} = \begin{cases} Z^{\otimes N} & \text{even integer} \\ -Z^{\otimes N} & \text{odd integer} \\ e^{-i\frac{\pi}{4}} I^{\otimes N} & \text{half-integer} \end{cases}. \tag{4.8}$$

[1] This can be easily verified via an explicit expansion of, for example, $(Z_1 + Z_2 + Z_3 + Z_4)^2$. Also, note the slight overworking of notation in this section coming from the composition of tensor products: for example, $Z_1 Z_2 := Z_1 \circ Z_2 = (\sigma_z \otimes I) \circ (I \otimes \sigma_z) = \sigma_z \otimes \sigma_z$

Appealing to the Hamiltonian symmetries, the work in [36] goes on to argue that the set of evolutions parameterized by the interval $\kappa \in [0, 2\pi j]$ contains a sort of reflection symmetry about $\kappa = j\pi$. In particular, that

$$U_\kappa \overset{\text{LO}}{\Longleftrightarrow} U_{\tilde{\kappa}}, \qquad \tilde{\kappa} \in [0, \pi j], \tag{4.9}$$

with the important caveat that the state on which the left-hand side of (4.9) acts upon is related to the state on which the right-hand acts upon via a collective spin-flip ($\theta \mapsto \pi - \theta$). We do not reproduce this result here but mention it to emphasize that the value $\kappa = j\pi$ is a significant one in the context of entanglement generation in the kicked top.

4.2 Temporal periodicity

In this section, we discuss the temporal periodicity of the kicked-top evolution. Unlike the global periodicity discussed in [36, 35] for spin-1, here we explore how the chaoticity parameter is related to unitary recurrence and its relationship to classical chaos.

The general expression for the twist unitary is

$$e^{-i\frac{\kappa}{2j}J_z^2} = e^{-i\frac{\kappa}{8j}N} \prod_{\vec{k}\neq 2} \left(I^{\otimes N} \cos\frac{\kappa}{4j} - iZ_1^{k_1} \cdots Z_N^{k_N} \sin\frac{\kappa}{4j} \right), \tag{4.10}$$

where $Z_k := \sigma_z^{(k)}$. It reduces to

$$e^{-i\frac{\pi}{2}J_z^2} = e^{-i\frac{\pi}{8}N} \prod_{\vec{k}\neq 2} \frac{1}{\sqrt{2}} \left(I^{\otimes N} - iZ_1^{k_1} \cdots Z_n^{k_N} \right) \tag{4.11}$$

This is a difficult expression to evaluate; therefore we want an alternative expression of this operator in qubit space. The proof for temporal periodicity in this case is of two parts. In the first part, we suggest an equivalent expression of the twist operator which is linear in J_z and then we prove the relation between the two. In the second part of the proof, we use this equivalent expression to show the temporal periodicity.

4.2.1 Twist strength $\kappa = j\pi$

The case of twist strength $\kappa = \pi j$ yields a more interesting temporal periodicity that also depends on the spin being an integer or half-integer.

Integer spin

For $\kappa = j\pi$ and integer value of j, we show that

$$e^{-i\frac{\pi}{2}J_z^2} = e^{-i\frac{\pi}{4}}\left[\frac{I^{\otimes N} + i(i\sigma_z)^{\otimes N}}{\sqrt{2}}\right] \tag{4.12}$$

by comparing the action of the two expressions on a computational basis.

Any N-qubit state with hamming weight k is written as

$$\left|D_N^{(k)}\right\rangle = \left|\underbrace{00\cdots0}_{N-k}\otimes\underbrace{1\cdots11}_{k}\right\rangle. \tag{4.13}$$

With this in mind, let's prove Eq. (4.12). Since any N-qubit state with the same hamming weight is an eigenstate of J_z with the same eigenvalue, the action of J_z can be written as,

$$J_z\left|D_N^{(k)}\right\rangle = \frac{(N-2k)}{2}\left|D_N^{(k)}\right\rangle. \tag{4.14}$$

$$J_z^2\left|D_N^{(k)}\right\rangle = \frac{(N-2k)^2}{4}\left|D_N^{(k)}\right\rangle. \tag{4.15}$$

$$e^{-i\frac{\pi}{2}J_z^2}\left|D_N^{(k)}\right\rangle = e^{-i\frac{\pi}{2}\frac{(N-2k)^2}{4}}\left|D_N^{(k)}\right\rangle. \tag{4.16}$$

Acting with right hand side of the Eq. (4.12) on the N-qubit ($\left|D_N^{(k)}\right\rangle$) state gives,

$$e^{-i\frac{\pi}{4}}\left[\frac{I^{\otimes N}+i(i\sigma_z)^{\otimes N}}{\sqrt{2}}\right]\left|D_N^{(k)}\right\rangle = e^{-i\frac{\pi}{4}}\left[\frac{I^{\otimes N}+(i)^{N+1}(\sigma_z)^{\otimes N}}{\sqrt{2}}\right]\left|D_N^{(k)}\right\rangle$$
$$= e^{-i\frac{\pi}{4}}\left[\frac{1+(i)^{N+1+2k}}{\sqrt{2}}\right]\left|D_N^{(k)}\right\rangle \tag{4.17}$$

Now we will show that Eq. (4.16) and Eq. (4.17) are equivalent, which implies the equation Eq. (4.12) holds,

$$e^{-i\frac{\pi}{2}\frac{(N-2k)^2}{4}} = e^{-i\frac{\pi}{4}}\left[\frac{1+(i)^{N+1+2k}}{\sqrt{2}}\right] \tag{4.18}$$

Since N is even, set $N = 2m$, where $m \in \{1, 2, ...\frac{N}{2}\}$. Therefore the left-hand side of Eq. (4.18) reduces to,

$$e^{-i\frac{\pi}{2}\frac{(N-2k)^2}{4}} = e^{-i\frac{\pi}{2}(m-k)^2}$$
$$= e^{-i\frac{\pi}{2}s^2} \tag{4.19}$$

where $s \in \{1, 2, ...m\}$. Here m and k can be odd or even. If k and m are both odd or even then s is an even number and otherwise s is an odd number. Therefore we get two solutions for the above case, i.e.,

$$e^{-i\frac{\pi}{2}\frac{(N-2k)^2}{4}} = \begin{cases} 1 & \text{when s is even, i.e., } (m-k) \text{ is even} \\ -i & \text{when s is odd, i.e., } (m-k) \text{ is odd} \end{cases} \tag{4.20}$$

Now, the right-hand side of the Eq. (4.18) takes the form,

$$e^{-i\frac{\pi}{4}}\left[\frac{1+(i)^{N+1+2k}}{\sqrt{2}}\right] = e^{-i\frac{\pi}{4}}\left[\frac{1+(i)^{2(m+k)+1}}{\sqrt{2}}\right] \tag{4.21}$$

where $m \in \{1, 2, ...\frac{N}{2}\}$. Since $(2(m+k)+1)$ is always an odd number, we can split it into two forms, $(4l+1)$, when both m and k are even or odd (i.e., $(m-k)$ is even), and $(4l-1)$ otherwise (i.e., $(m-k)$ is odd) which results in,

$$(i)^{N+1+2k} = \begin{cases} +i & \text{when } 2(m+k)+1 = 4l+1 \\ -i & \text{when } 2(m+k)+1 = 4l-1 \end{cases} \tag{4.22}$$

Therefore in this case we get two solutions as well which are of form

$$e^{-i\frac{\pi}{4}}\left[\frac{1+(i)^{N+1+2k}}{\sqrt{2}}\right] = \begin{cases} 1 & \text{when } 2(m+k)+1) = 4l+1, \text{ i.e., } (m-k) \text{ is even} \\ -i & \text{when } 2(m+k)+1) = 4l-1, \text{ i.e., } (m-k) \text{ is odd} \end{cases} \tag{4.23}$$

Since the solutions of Eq. (4.20) and Eq. (4.23) are the same, the relation in Eq. (4.12) is proved.

In the second part of the proof we now show that the Floquet operator shows temporal periodicity. This can be done through repeated use of the Pauli group commutation relations. For any two elements g and h of a group G, a commutation relation is defined as

$$[g, h] := g^{-1}h^{-1}gh \tag{4.24}$$

First, we define the rotation part of the Floquet operator as

$$e^{-ipJ_y} = (I\cos\frac{p}{2} - i\sigma_y \sin\frac{p}{2})^{\otimes N} \tag{4.25}$$

for $p = \frac{\pi}{2}$, the above expression reduces to

$$\gamma^{\otimes N} := e^{-i\frac{\pi}{2}J_y} = (I\cos\frac{\pi}{4} - i\sigma_y \sin\frac{\pi}{4})^{\otimes N}. \tag{4.26}$$

Therefore the commutation relation between γ and σ_z is given as

$$\begin{aligned}[\sigma_z, \gamma] &= \sigma_z^{-1}\gamma^{-1}\sigma_z\gamma \\ &= i\sigma_y \end{aligned} \tag{4.27}$$

This implies

$$\sigma_z\gamma = -\gamma\sigma_x \tag{4.28}$$

Similarly,

$$\sigma_x\gamma = \gamma\sigma_z \tag{4.29}$$

We will use the above relations for our upcoming proofs. To show the temporal periodicity, we will take the fourth power of the full unitary and compute its irreducible form.

$$\begin{aligned}
U_{\pi j}^4 &= \left[\frac{e^{-i\frac{\pi}{4}}}{\sqrt{2}}\left(I^{\otimes N} + i(i\sigma_z)^{\otimes N}\right)\left(\frac{I - i\sigma_y}{\sqrt{2}}\right)^{\otimes N}\right]^4 \\
&= \frac{e^{-i\pi}}{4}\left[\left((I^{\otimes N} + i(i\sigma_z)^{\otimes N})\gamma^{\otimes N}\right)\right]^4 \\
&= \frac{e^{-i\pi}}{4}\left[(I^{\otimes N} + i(i\sigma_z)^{\otimes N})\left((I^{\otimes N} + i(i\sigma_x)^{\otimes N})\gamma^{\otimes N}\right)^3\right]\gamma^{\otimes N} \\
&= \frac{e^{-i\pi}}{4}\left[(I^{\otimes N} + i(i\sigma_z)^{\otimes N})(I^{\otimes N} + i(i\sigma_x)^{\otimes N})\left((I^{\otimes N} + i(i\sigma_z)^{\otimes N})\gamma^{\otimes N}\right)^2\right](\gamma^{\otimes N})^2 \\
&= \frac{e^{-i\pi}}{4}\left[(I^{\otimes N} + i(i\sigma_z)^{\otimes N})(I^{\otimes N} + i(i\sigma_x)^{\otimes N})(I^{\otimes N} + i(i\sigma_z)^{\otimes N})(I^{\otimes N} + i(i\sigma_x)^{\otimes N})\right](\gamma^{\otimes N})^4 \\
&= \frac{e^{-i\pi}}{4}\left[(I^{\otimes N} + i(i\sigma_x)^{\otimes N} + i(i\sigma_z)^{\otimes N} - (i\sigma_y)^{\otimes N})\right]^2(-1). \qquad (\because (\gamma^{\otimes N})^4 = -\mathbb{I}) \\
&= \frac{-e^{-i\pi}}{4}\left[-4(i\sigma_y)^{\otimes N})\right]. \\
&= -(i\sigma_y)^{\otimes N}
\end{aligned} \tag{4.30}$$

Therefore

$$U_{\pi j}^{4} = \left[\frac{e^{-i\frac{\pi}{4}}}{\sqrt{2}} (I^{\otimes N} + i(i\sigma_z)^{\otimes N}) \frac{1}{\sqrt{2}} (I - i\sigma_y)^{\otimes N} \right]^4 = -(i\sigma_y)^{\otimes N} \tag{4.31}$$

Using the above relation, we show that the Floquet operator exhibits the finite-time periodicity

$$U_{\pi j}^{8} = I \qquad \forall \text{ integer } j. \tag{4.32}$$

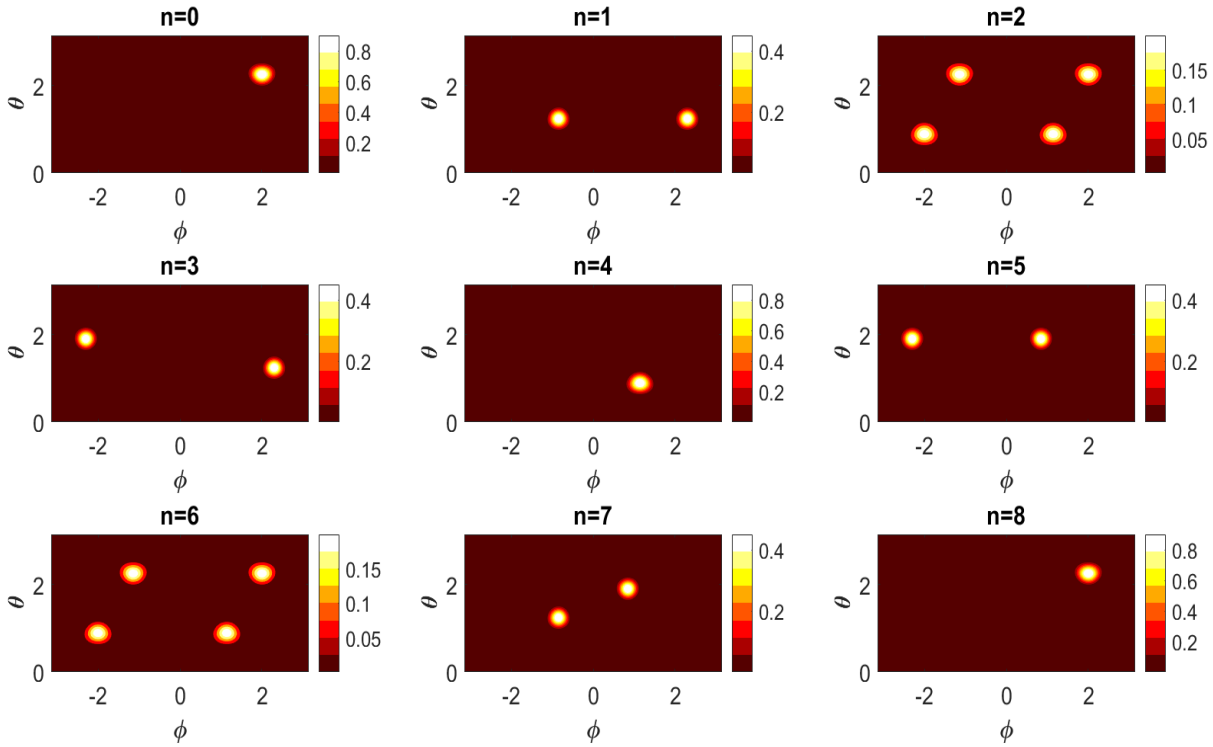

Figure 4.1: The Husimi plot of the system with $j = 50$ and $\kappa = j\pi$. Here it can be seen that after every 8 kicks state returns to its initial state, thus showing the temporal periodicity of 8 kicks. Initial state is centred at $(\theta, \phi) = (2.25, 2.0)$.

The effect of the above relation, Eq. (4.55) can be seen on a spin-coherent state in Fig. 4.1. We show the Husimi plot for $j = 50$ system with the initial state as $\theta = 2.25$ and $\phi = 2.0$. At this value of κ, after applying the rotation, the kick part of the unitary

(Eq. 4.12), splits the state into two and creates the equal superposition of the two spin coherent states. On applying the second rotation, the state gets rotated by $\pi/2$ along the y-axis. Kicking it again with the non-linear part of the unitary splits the state again and creates an equal superposition of four spin coherent states. Further action of the unitary recombines the superposition of four to two spin coherent states. Moreover, after the four kicks, the state again becomes a spin-coherent state but gets rotated by π along the y-axis. On applying the unitary for another four times, the dynamics just retrace the previous path on the phase space, and thus, after every eight kicks system returns to its initial state. It should be noted that it is the combined effect of rotation and kick part that we get $U^8 = \mathbb{1}_{2j}$, and thus any initial spin coherent state centered at $|\theta, \phi\rangle$ will show similar behavior. It should also be noted that while the above is the generic temporal periodicity, certain states related to the Hamiltonian symmetries will experience a shorter orbit. In particular if we take the initial state as $|+\rangle_y$, i.e. $(\theta, \phi) = (\pi/2, \pi/2)$, then the rotation part of the unitary will be ineffective. The twist (4.12) will create the superposition of $|+\rangle_y$ and $|-\rangle_y$; it can be shown that the evolution reduces to a period-4 orbit for even integer spins and a period-2 orbit for odd integer spins. However, at the end of every eight kicks, any spin coherent state centered at any point on the phase space returns to its original state.

Half-integer spin

In the case of half-integer spin and $\kappa = j\pi$, the general twist operator(Eq. (4.10)), happens to be equivalent to the following unitary in the qubit picture:

$$e^{-i\frac{\pi}{2}J_z^2} = \frac{e^{-i\frac{\pi}{8}}}{\sqrt{2}}\left[e^{i\frac{\pi}{2}J_z} + e^{-i\frac{\pi}{2}J_z}\right] \tag{4.33}$$

$$= \frac{e^{-i\frac{\pi}{8}}}{\sqrt{2}}\left[\left(\frac{I+iZ}{\sqrt{2}}\right)^{\otimes N} + \left(\frac{I-iZ)}{\sqrt{2}}\right)^{\otimes N}\right]. \tag{4.34}$$

In this case, as well, we show the equivalence relation by its action on N-qubit basis

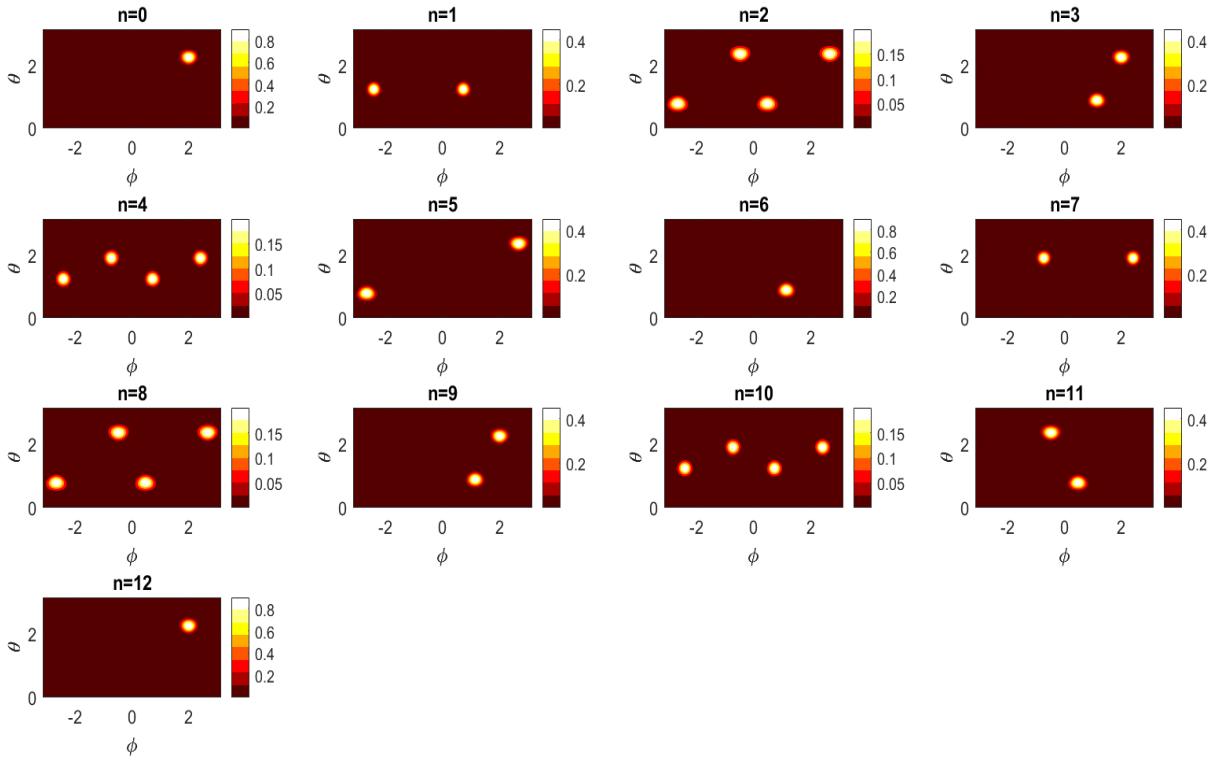

Figure 4.2: The Husimi plot of the system with $j = 50.5$ and $\kappa = j\pi$. Here it can be seen that after every 12 kicks state returns to its initial state, thus showing the temporal periodicity of 12 kicks. Initial state is centred at $(\theta, \phi) = (2.25, 2.0)$.

states. Again the twist operator acts in the same way as Eq. (4.16). The right-hand side on Eq. (4.33) acts in the following way

$$e^{-i\frac{\pi}{8}}\frac{1}{\sqrt{2}}\left[e^{i\frac{\pi}{2}J_z}+e^{-i\frac{\pi}{2}J_z}\right]\left|D_N^{(k)}\right\rangle = e^{-i\frac{\pi}{8}}\frac{1}{\sqrt{2}}\left[e^{i(N-2k)\frac{\pi}{4}}+e^{-i(N-2k)\frac{\pi}{4}}\right]\left|D_N^{(k)}\right\rangle, \tag{4.35}$$

Eq. (4.33) and Eq. (4.35) imply,

$$e^{-i\frac{\pi}{2}\frac{(N-2k)^2}{4}} = e^{-i\frac{\pi}{8}}\frac{1}{\sqrt{2}}\left[e^{i(N-2k)\frac{\pi}{4}}+e^{-i(N-2k)\frac{\pi}{4}}\right] \tag{4.36}$$

To prove the above relations, let's first consider the left-hand side of Eq. (4.36). Since

N is odd and $2k$ is even, $(N-2k)$ will always be odd and it will vary from $-N$ to N. Therefore, $(N-2k)^2$ will vary from 1 to N^2. Define m such that

$$N - 2k := 2m + 1 \tag{4.37}$$

where $m \in \{0, 1, 2, .., \frac{N-1}{2}\}$. Therefore,

$$\begin{aligned} e^{-i\frac{\pi}{2}\frac{(N-2k)^2}{4}} &= e^{-i\frac{\pi}{2}\frac{(2m+1)^2}{4}} \\ &= e^{-i\frac{\pi}{8}} e^{-i\frac{\pi m(m+1)}{2}} \end{aligned} \tag{4.38}$$

Here it can be seen that Eq. (4.38) takes a value $e^{-i\frac{\pi}{8}}\{1, -1, -1, 1\}$ for $m = \{0, 1, 2, 3\}$ and it is the same for m mod 4.

Now consider the right-hand side of the Eq. (4.36). It can be written as

$$e^{-i\frac{\pi}{8}} \frac{1}{\sqrt{2}} \left[e^{i(N-2k)\frac{\pi}{4}} + e^{-i(N-2k)\frac{\pi}{4}} \right] = e^{-i\frac{\pi}{8}} \frac{1}{\sqrt{2}} \left[2\cos((N-2k)\frac{\pi}{4}) \right] \tag{4.39}$$

where $(N-2k) \in \{-N, N+1, ...N\}$. Since *cosine* is an even function and $(N-2k)$ is odd of the form $(2m+1)$, the argument of the *cosine* function only varies from 1 to N.

$$e^{-i\frac{\pi}{8}} \frac{1}{\sqrt{2}} \left[e^{i(N-2k)\frac{\pi}{4}} + e^{-i(N-2k)\frac{\pi}{4}} \right] = e^{-i\frac{\pi}{8}} \frac{1}{\sqrt{2}} \left[2\cos((2m+1)\frac{\pi}{4}) \right] \tag{4.40}$$

Here also it can be seen that Eq. (4.40) takes a value $\{1, -1, -1, 1\}$ for $m = \{0, 1, 2, 3\}$ and it is same for m mod 4. Therefore, the proof of Eq. (4.36) is complete.

To show the temporal periodicity of the full floquet operator, we will use the expression of the twist operator given in Eq. (4.33) along with the rotation part of the unitary given by Eq. (4.26) and we consider its sixth power

$$U^6_{\pi j} = \left[e^{-i\frac{\pi}{8}} \frac{1}{\sqrt{2}} \left(e^{i\frac{\pi}{2}J_z} + e^{-i\frac{\pi}{2}J_z} \right) \gamma^{\otimes N} \right]^6 \tag{4.41}$$

We use a similar trick as in the integer-spin case of pulling the rotation part of U^6 to the end using group commutator relations. This leads us to

$$\begin{aligned} U^6_{\pi j} &= \frac{e^{-i\frac{3\pi}{4}}}{8} \left[\left(e^{i\frac{\pi}{2}J_y} + e^{-i\frac{\pi}{2}J_y} \right) \left(e^{i\frac{\pi}{2}J_z} + e^{-i\frac{\pi}{2}J_z} \right) \right]^3 (\gamma^{\otimes N})^6 \\ &= \frac{e^{-i\frac{3\pi}{4}}}{8} A^3 (i\sigma_y)^{\otimes N}. \end{aligned} \tag{4.42}$$

where A is composed of the terms inside the square brackets. Now we compute A^2 and we show that A^3 reduces to $\mathbb{I}$ with some coefficient. In the next few steps we repeatedly used the following relations,

$$e^{+i\frac{\pi}{2}J_b}\, e^{-i\theta J_a}\, e^{-i\frac{\pi}{2}J_b} = \epsilon_{abc}\, e^{-i\theta J_c} \qquad \text{where } (a,b,c) \in (x,y,z) \tag{4.43}$$

and

$$\left(e^{\pm i\frac{\pi}{2}J_a}\, e^{\pm i\frac{\pi}{2}J_b} \right)^3 = -\mathbb{I} \qquad \text{where } (a,b) \in (x,y,z). \tag{4.44}$$

Let's write A^2 as

$$A^2 = \left[e^{+i\frac{\pi}{2}J_y} e^{+i\frac{\pi}{2}J_z} + e^{+i\frac{\pi}{2}J_y} e^{-i\frac{\pi}{2}J_z} + e^{-i\frac{\pi}{2}J_y} e^{+i\frac{\pi}{2}J_z} + e^{-i\frac{\pi}{2}J_y} e^{-i\frac{\pi}{2}J_z} \right]^2.$$

using Eq. (4.43) and Eq. (4.44) in the above expression we get

$$\begin{aligned} A^2 = {} & (e^{-i\frac{\pi}{2}J_y} e^{-i\frac{\pi}{2}J_z})^2 + 2(e^{+i\frac{\pi}{2}J_y} e^{+i\frac{\pi}{2}J_x}) + 2(e^{+i\frac{\pi}{2}J_x} e^{+i\frac{\pi}{2}J_z}) \\ & + 2(e^{+i\frac{\pi}{2}J_x} e^{-i\frac{\pi}{2}J_z}) + (e^{+i\frac{\pi}{2}J_y} e^{-i\frac{\pi}{2}J_z})^2 + (e^{-i\frac{\pi}{2}J_y} e^{-i\frac{\pi}{2}J_x}) \\ & + 2(e^{-i\frac{\pi}{2}J_x} e^{-i\frac{\pi}{2}J_z})^2 + (e^{-i\frac{\pi}{2}J_x} e^{+i\frac{\pi}{2}J_z}) + (e^{-i\frac{\pi}{2}J_y} e^{+i\frac{\pi}{2}J_z})^2 \\ & + (e^{-i\frac{\pi}{2}J_y} e^{+i\frac{\pi}{2}J_x}) + (e^{-i\frac{\pi}{2}J_y} e^{-i\frac{\pi}{2}J_x})^2 + (e^{-i\frac{\pi}{2}J_y} e^{-i\frac{\pi}{2}J_z})^2. \end{aligned} \tag{4.45}$$

Multiplying the above expression with A, we get,

$$A^3 = 8\,\mathbb{I}. \tag{4.46}$$

Using Eq. (4.41) and Eq. (4.46) we get

$$U_{\pi j}^{6} = e^{-i\frac{3\pi}{4}}(i\sigma_y)^{\otimes N}. \tag{4.47}$$

Finally,

$$U_{\pi j}^{12} = e^{-i\frac{\pi}{2}}\mathbb{I}. \tag{4.48}$$

Similar to the case of an integer-spin, in the case of a half-integer we observe the splitting of the initial spin-coherent state. After six kicks we see an effective rotation along the y-axis by an angle π. Fig 4.2 shows the evolution of an initial state for $j = 50.5$. The plot shows the splitting of the states taking place, and after every 12 kicks the states recombine (instead of 8 kicks), as seen in the case of integer spin. States associated with Hamiltonian symmetries again experience a reduced orbit length. For the initial state as $|+\rangle_y$, i.e. $(\theta, \phi) = (\pi/2, \pi/2)$, the evolution reduces to a period-3 orbit.

4.2.2 Twist strength $\kappa = 2j\pi$

The Floquet operator in the case of $\kappa = 2j\pi$ is

$$U_{2\pi j} = e^{-i\pi J_z^2} e^{-ipJ_y}, \tag{4.49}$$

where $e^{-i\pi J_z^2}$ is a symmetric local unitary in the qubit picture. The consequence of this on any temporal periodicity strongly depends on whether the spin is an integer or a half-integer.

Integer spin

In the case of integer spin the evolution squares to the identity regardless of the y-rotation angle: $U_{2\pi j}^2 = I^{\otimes n}$. This can be seen by using the integer forms of Eq. (4.8).

As $U_{2\pi j}^2$ is a composition of symmetric local unitaries it suffices to consider a single tensor factor:

$$[Z(I\cos\frac{p}{2} - iY\sin\frac{p}{2})]^2 = [Z\cos\frac{p}{2} - X\sin\frac{p}{2}]^2 = I. \tag{4.50}$$

See Fig. 4.3 for a visual interpretation through tracking the shared Bloch vector. After the first y-rotation the twist effectively acts as a π-rotation about the z axis. Consequently, the second y-rotation undoes the first and the final twist rotates back to the starting point. Note that because each step in this process is a rigid rotation any initial spin coherent state will remain so throughout, and no correlations are generated.

Half-integer spin

In the case of half-integer spin the twist becomes a scaled identity operator, leading to a temporal periodicity up to the global phase of N kicks under the condition

$$I = e^{-ipNJ_y} \quad \Rightarrow \quad N = \frac{2\pi}{p}. \tag{4.51}$$

Thus only when p is a rational fraction of π does there exist a temporal periodicity. Regardless however of the value of p, the evolution of a state is only via a set of rotations along one axis.

It is interesting to see that in the half-integer case, the rotation angle p is critical for determining the existence of a temporal periodicity while in the integer case, p has no effect. In both cases, as expected due to the lack of entanglement, the evolutions are not ergodic in the sense of exploring Hilbert space.

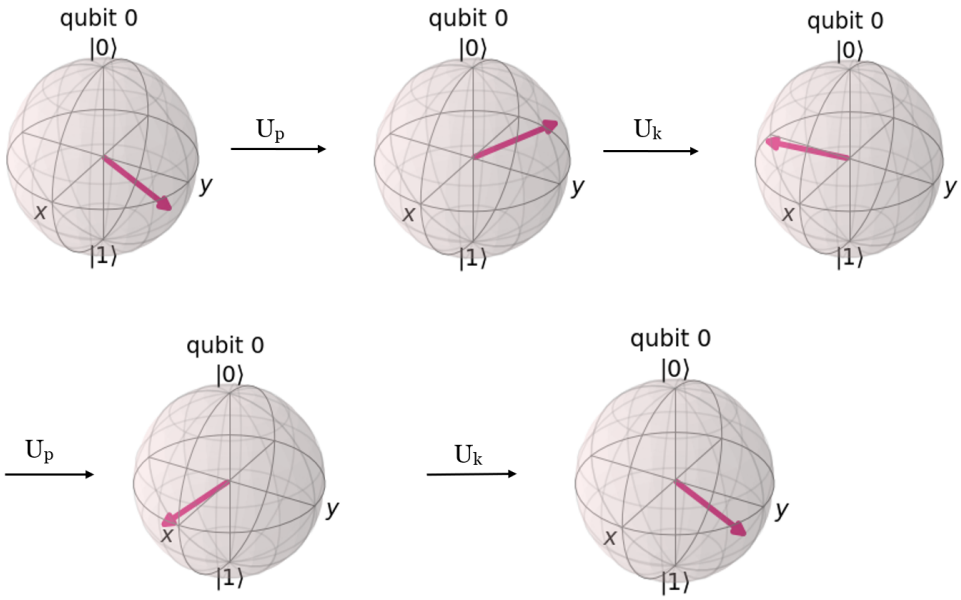

Figure 4.3: Evolution of the Bloch vector associated to any reduced qubit state of full state with even number of qubits for $\kappa = 2j\pi$. After two kicks the state returns to its initial point, showing a two-step temporal periodicity. The initial point is $(\theta, \phi) = (2.25, 2.0)$.

4.2.3 Twist strength $\kappa = 3j\pi$

The case of twist strength $\kappa = 3\pi j$ is easy to evaluate as it can be viewed as a composition of the previous two cases. In this case, the twist operator takes the form

$$\begin{aligned} e^{-i\frac{\kappa}{2j}J_z^2} &= e^{-i\frac{3\pi}{2}J_z^2} \\ &= e^{-i\pi J_z^2}\, e^{-i\frac{\pi}{2}J_z^2} \\ &= U_{\kappa=2\pi j}\, U_{\kappa=\pi j}. \end{aligned} \tag{4.52}$$

Here, $U_{\kappa=2\pi j}$ and $U_{\kappa=\pi j}$ refer to the twist part of the unitary for the corresponding κ values. Similar to the case of $\kappa = j\pi$, the integer and half-integer spin will behave

differently in this case as well. However, the periodicity will be the same as that of $\kappa = j\pi$.

Integer spin

For the integer spin, the twist operator can be written as

$$\begin{aligned} e^{-i\frac{3\pi}{2}J_z^2} &= U_{\kappa=2\pi j}\, U_{\kappa=\pi j} \\ &= (-1)^j\, \sigma_z^{\otimes n}\, e^{-i\frac{\pi}{4}} \left[\frac{I^{\otimes N} + i(i\sigma_z)^{\otimes N}}{\sqrt{2}}\right]. \end{aligned} \tag{4.53}$$

The full Floquet operator is given by

$$\begin{aligned} U_{3\pi j} &= \left[U_{\kappa=2\pi j}\, U_{\kappa=\pi j}\right] \left[\frac{1}{\sqrt{2}}(I - i\sigma_y)^{\otimes N}\right] \\ &= (-1)^j\, \sigma_z^{\otimes n}\, e^{-i\frac{\pi}{4}} \left[\frac{I^{\otimes N} + i(i\sigma_z)^{\otimes N}}{\sqrt{2}}\right] \frac{1}{\sqrt{2}}(I - i\sigma_y)^{\otimes N} \\ &= (-1)^j\, e^{-i\frac{\pi}{4}} \left[\frac{\sigma_z^{\otimes N} + i^{N+1} I^{\otimes N}}{\sqrt{2}}\right] \gamma^{\otimes N}. \end{aligned} \tag{4.54}$$

Now, taking the fourth power of the Floquet operator and using the same technique of group commutators relations, we get

$$U_{3\pi j}^4 = e^{-i\pi}\, (i\sigma_y)^{\otimes N}$$

This gives us the periodicity for this case as

$$U_{3\pi j}^8 = \mathbb{I} \qquad \forall \text{ integer } j. \tag{4.55}$$

Half-Integer spin

For the case of half-integer spin, we can write the Floquet operator as

$$\begin{aligned} U_{3\pi j} &= U_{\kappa=2\pi j}\, U_{\kappa=\pi j} \\ &= \left[e^{-i\frac{\pi}{4}} I^{\otimes N}\right]\left[\frac{e^{-i\frac{\pi}{8}}}{\sqrt{2}}\left[\left(\frac{I+iZ}{\sqrt{2}}\right)^{\otimes N}+\left(\frac{I-iZ)}{\sqrt{2}}\right)^{\otimes N}\right]\right]\gamma^{\otimes N} \\ &= \frac{e^{-i\frac{3\pi}{8}}}{\sqrt{2}}\left[\left(\frac{I+iZ}{\sqrt{2}}\right)^{\otimes N}+\left(\frac{I-iZ)}{\sqrt{2}}\right)^{\otimes N}\right]\gamma^{\otimes N}. \end{aligned} \tag{4.56}$$

where the twist part is written using Eq. (4.8) and Eq. (4.33). Using similar techniques as in the case of $\kappa = j\pi$, we get the 12-th power of the full Floquet operator as

$$U_{3\pi j}^{12} = e^{-i\frac{\pi}{2}}\mathbb{I}. \tag{4.57}$$

Therefore, for $\kappa = 3j\pi$, the Floquet operator has the same periodicity as for $\kappa = j\pi$ for both integer and half-integer spin.

4.2.4 Twist strength $\kappa = j\frac{\pi}{2}$

Let us now investigate the case of $\kappa = \frac{j\pi}{2}$. Here the difference between integer and half-integer spin is strongest, though the results are entirely numerical.

Integer spin

Using the Gaussian sum decomposition [83], for integer spin the twist operator $e^{-i\frac{\pi}{4}J_z^2}$ splits into the superposition of rotations

$$\frac{1}{2}\left[e^{-i\frac{\pi}{4}} I + e^{-i\frac{\pi}{2}J_z} + e^{i\frac{3\pi}{4}} e^{-i\pi J_z} + e^{-i\frac{3\pi}{2}J_z}\right]. \tag{4.58}$$

In the qubit picture this becomes

$$e^{-i\frac{\pi}{4}J_z^2} = \frac{1}{2}\Bigg[e^{-i\frac{\pi}{4}}I^{\otimes n} + \left(\frac{I-iZ}{\sqrt{2}}\right)^{\otimes n} \\ e^{i\frac{3\pi}{4}}(iZ)^{\otimes n} + \left(\frac{I+iZ}{\sqrt{2}}\right)^{\otimes n}\Bigg] \tag{4.59}$$

where we have used the fact that n is even to simplify. Numerical calculations suggest a temporal periodicity with period 48,

$$U_{\frac{\pi j}{2}}^{48} = I \qquad \forall \text{ integer } j. \tag{4.60}$$

This has been confirmed up to spin $j = 500$ where the Hilbert–Schmidt distance $\|U_{\frac{\pi j}{2}}^{48} - I\|$ remains zero within the working error tolerance of 10^{-10}. And similar to the previous $\kappa = \pi j$ case (both integer and half-integer) here the Floquet operator raised to half the periodicity (i.e. 24) also acts as an effective π-rotation about the y-axis up to some global phase. Cat-like splitting and recombination cycles were furthermore observed in the Husimi function tracking of a generic spin coherent state. Part of the difficulty in showing this analytically comes from determining the twist operator in the qubit picture as in Eqs. (4.12) and (4.33). Numerics also confirm a period-48 recurrence at $\kappa = \frac{\pi j}{2} + 2\pi j = \frac{5\pi j}{2}$.

We also note what appears to be two accidental temporal recurrences present in low dimensions at this chaoticity value; for $j = 1$ and $j = 3$ the evolution repeats after only 16 kicks rather than 48. This observation is distinct from the continued theme of the special states $|\pm\rangle_y$ experiencing a reduced orbit of 24 for even values of j and 4 for odd values of j which we numerically verified.

Half-integer spin

In the half-integer case we surprisingly find no temporal periodicity for $\kappa = \frac{\pi j}{2}$. This was numerically concluded by computing the entanglement entropy of any one of the

reduced constituent qubits,

$$\rho = \frac{1}{2}\begin{pmatrix} 1-\langle S_z\rangle & \langle S_-\rangle \\ \langle S_+\rangle & 1+\langle S_z\rangle \end{pmatrix}, \tag{4.61}$$

via the collective spin observables $\{S_z, S_\pm = S_x \pm iS_y\}$ where $S_i = J_i/j$ [**?**]. This approach was used instead of Hilbert-Schmidt distance to avoid optimizing over the angles φ that could have *a priori* appeared in a hypothetical periodicity of the form $U^n = e^{i\varphi} I$.

All that is needed to conclude the lack of a global recurrence is the identification of a spin coherent state that never returns to product form. We thus focus on our running example of $|\theta, \phi\rangle = |2.25, 2.0\rangle$. We found that up to spin $j = 50\frac{1}{2}$ the single qubit dynamical entropy never falls below 10^{-5} within the first 5000 kicks. In fact, the entropy generally increased with dimension. Fig. 4.4 plots the *smallest* entanglement entropy obtained by any of qubits throughout the first 5000 kicks. As can be seen, higher spins experience a highly entangled orbit, remaining close to the upper bound of $S_{\max} = \ln 2$.

Further evidence supporting the lack of a recurrence can be found in the specific case of spin $j = \frac{3}{2}$, the smallest possible kicked top applicable to this scenario. Recently, many aspects of this low-dimensional system were solved exactly, including the single-qubit linear entropy

$$S_\rho^{(\mathrm{lin})} = 1 - \mathrm{Tr}\left[\rho^2\right] \tag{4.62}$$

of various initial spin states as a function of twist strength and kick number n [37]. In particular, the single-qubit linear entropy of the state $U_\kappa^n |+\rangle_y$ was found to be

$$S^{(\mathrm{lin})}(n, \kappa) = 4\chi^2 U_{n-1}^2(\chi)[1 - 2\chi^2 U_{n-1}^2(\chi)], \tag{4.63}$$

where

$$U_{n-1}(\chi) = \frac{\sin(n\gamma)}{\sin(\gamma)} \tag{4.64}$$

are the Chebyshev polynomials with arguments related to the twist strength via

$$\chi = \cos(\gamma) = \frac{1}{2}\sin\left(\frac{\kappa}{3}\right). \tag{4.65}$$

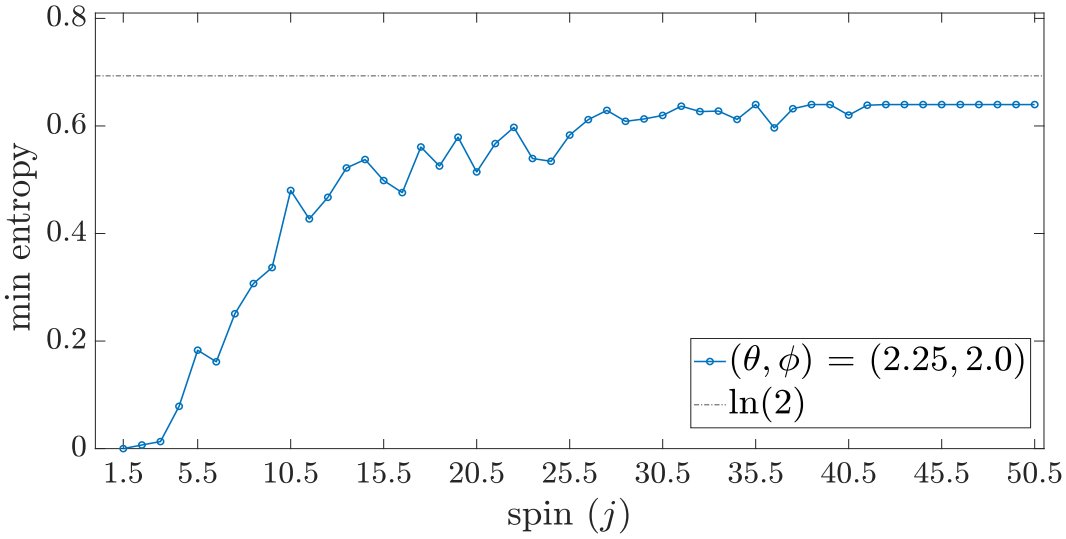

Figure 4.4: Minimum single-qubit entropy within the first 5000 kicks at $\kappa = \frac{\pi j}{2}$ as a function of spin. Initial spin coherent state is centred at $(\theta, \phi) = (2.25, 2.0)$.

Eq. (4.63) may be efficiently computed using symbolic programming and we found that the linear entropy does not exactly vanish within the first million kicks.

Given that a recurrence is almost certainly not present in the $j = 3/2$ system at this twist strength, it seems highly unlikely that a family of recurrences exist, one for each half-integer $j > 3/2$. This argument has an added strength by focusing on the special state $|+\rangle_y$, which, due to the Hamiltonian symmetry of the system, has a history of experiencing a reduced recurrence time when a global periodicity exists.

The lack of periodicity at this κ value also shows that in general, not all twist strengths commensurate to π yield an exact recurrence.

4.2.5 Landscape of periodicity

As mentioned in Sec. 4.1, the full Floquet operator remains invariant under the transformation, $\kappa \to \kappa + 4j\pi$, i.e., $U_\kappa = U_{\kappa+4j\pi}$. This results in identical dynamics for any initial state on the transformation of $4j\pi$ in κ values. So the dynamics are similar

for $\kappa = 0$ and $\kappa = 4j\pi$. Therefore we get a unique evolution of quantum states only up to $4j\pi$. Table 4.1 summarizes our results. With these recurrences established, a natural question to ask is if there are others. To this end, we have performed a numerical search for such recurrences characterized by $\kappa = \pi j\frac{r}{s}$ for all coprime $1 \leq r, s \leq 10$, and have found none. This was done by computing the $\|U^N_{\kappa=\pi j\frac{r}{s}} - I\|$ for the different sets of r ans s, with $j = 15$ and $j = 15.5$ upto 500 kicks. Numerical simulations suggests that there are no other sets of r and s that shows the temporal periodicity, than what we have found. This therefore places constraints on any additional values of κ that yield a state-independent finite periodicity.

In the range $(0, 4j\pi)$, we have considered κ of the form $mj\frac{\pi}{2}$. For all even values of m, we have analytically calculated the periodicity in the previous section. For all the odd values of m, our numerical simulations suggest that for the integer-spin system, $U^{48} = \mathbb{I}$. The periodicities of different κ values are given in Table 4.1 below. For a given κ and j, if κ mod $4j\pi$ is one of the values listed in the table, then the system will show the periodicity. In Fig. 4.5 we have taken κ as integer and half-integer multiples of π and different system sizes ranging from 1 to 100 spin values. The different colours show different periodicities. Here, it can be seen that for a given value of κ, as we increase system size, the transition from quantum to classical is not smooth. It should be noted that the special κ for different values of j shown in Fig.4.5 are the ones we found in our study. There may be other values for which the correspondence does not hold and thus the hunt for other special parameters continues.

4.3 Stability analysis

In the previous section we showed that for certain values of the chaoticity parameter κ, the quantum kicked top unitary acquires a temporal periodicity, and therefore does not reflect the classical dynamics, chaotic or otherwise. Here we discuss the stability of these special parameters via perturbations of the form $\tilde{\kappa} = \kappa + \delta$, where $\tilde{\kappa}$ is one of the above special values and δ is some small deviation.

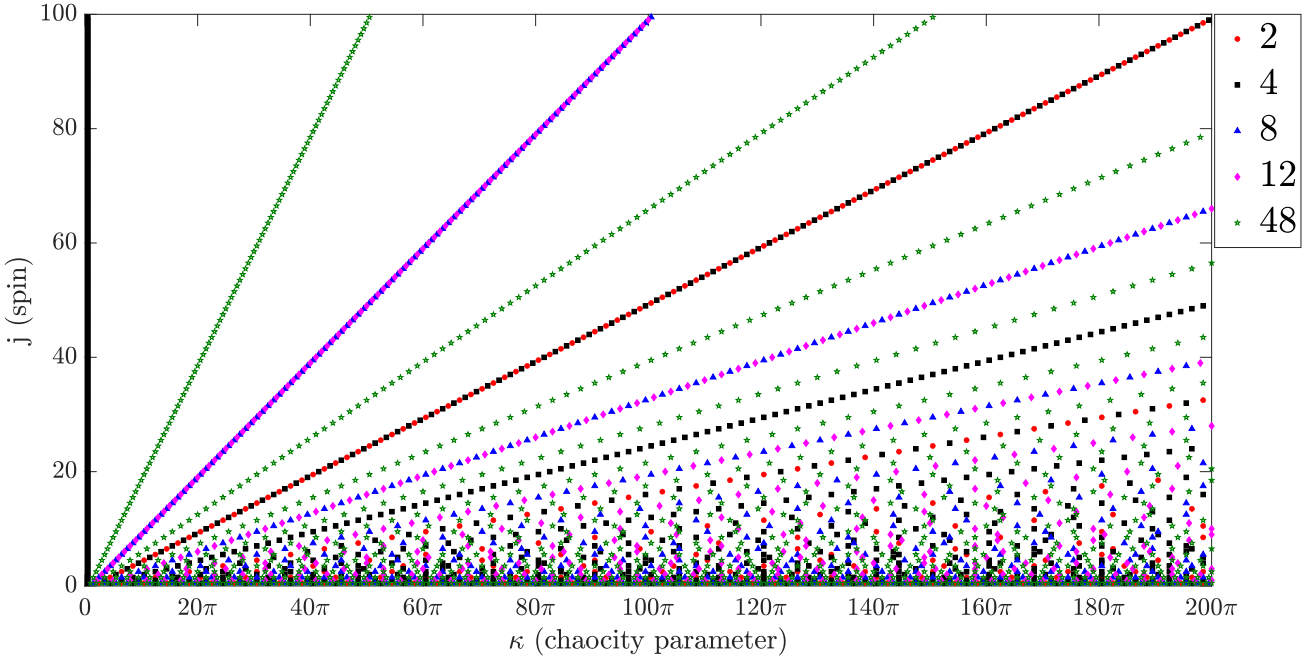

Figure 4.5: Here we have taken integer and half-integer values of j and κ. We calculated the set of j and κ for which we observe the anomalous periodicity.

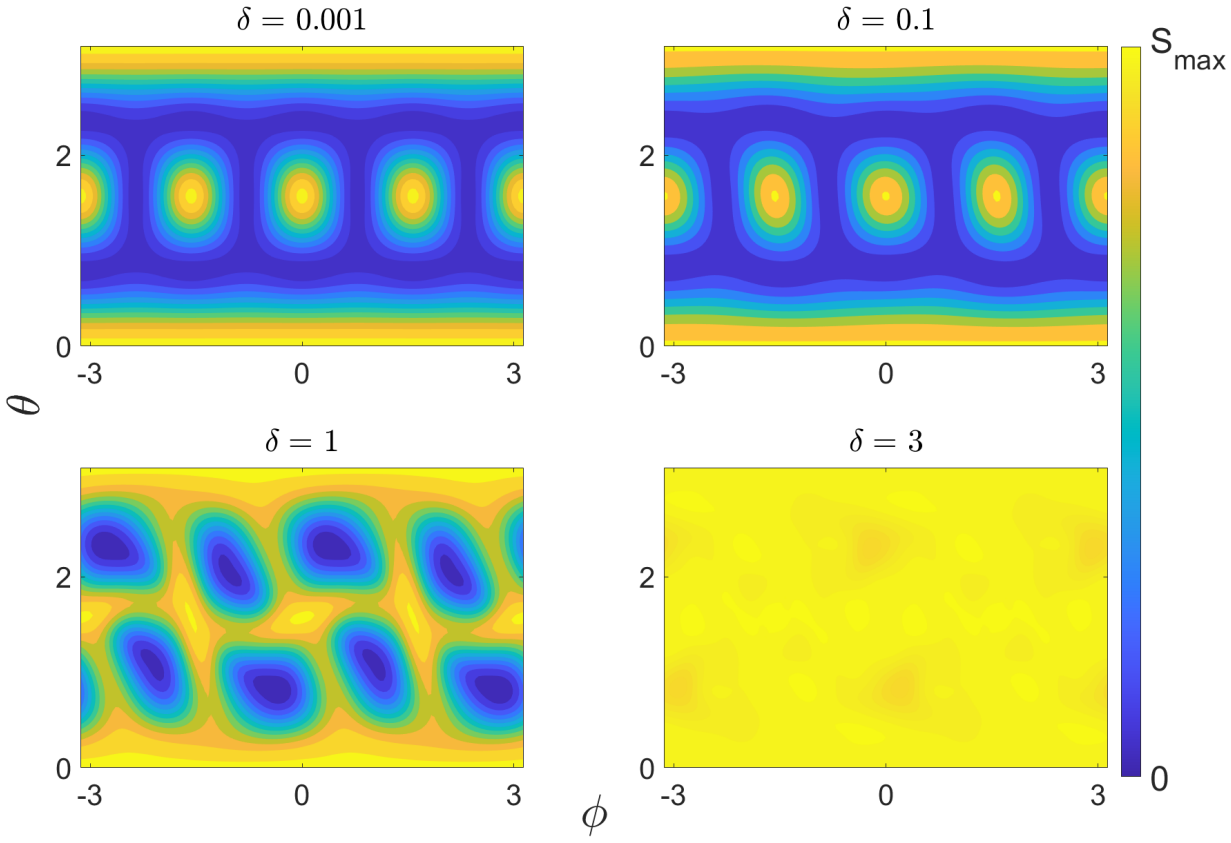

Figure 4.6: Average entanglement entropy with $j = 25.5$ and $\kappa = \pi j + \delta$, calculated on a grid of 70 x 140 initial spin coherent states. Each initial state is time-averaged over 10 applications of $U^{12}_{\pi j+\delta}$ to see the cumulative effect of the error δ. $S_{max} = \{7 \times 10^{-11}, 2 \times 10^{-3}, 0.6097, 0.6868\}$ is the maximum time average entanglement entropy, for $\delta = \{0.001, 0.1, 1, 3\}$, respectively.

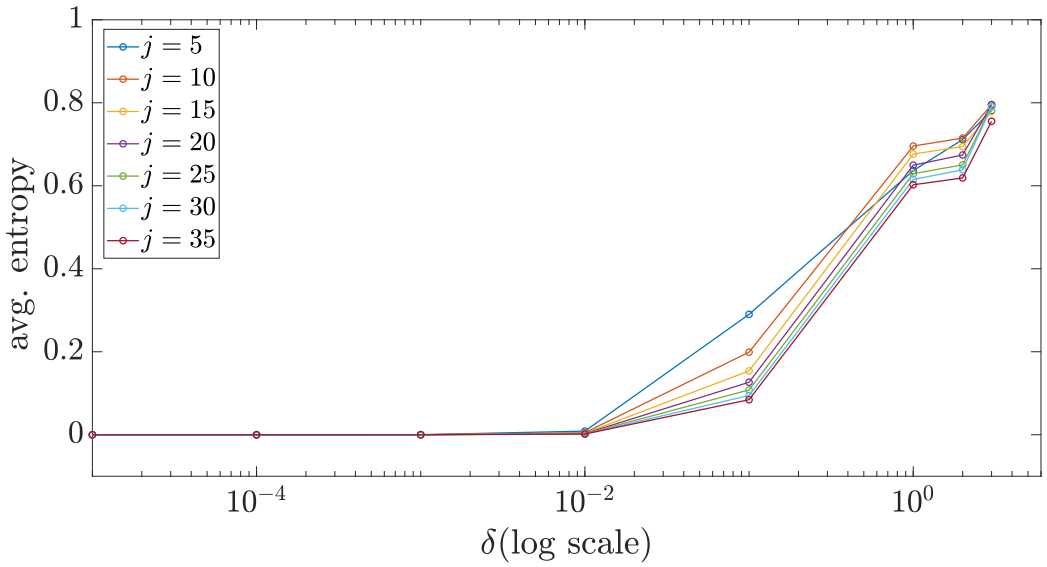

(a)

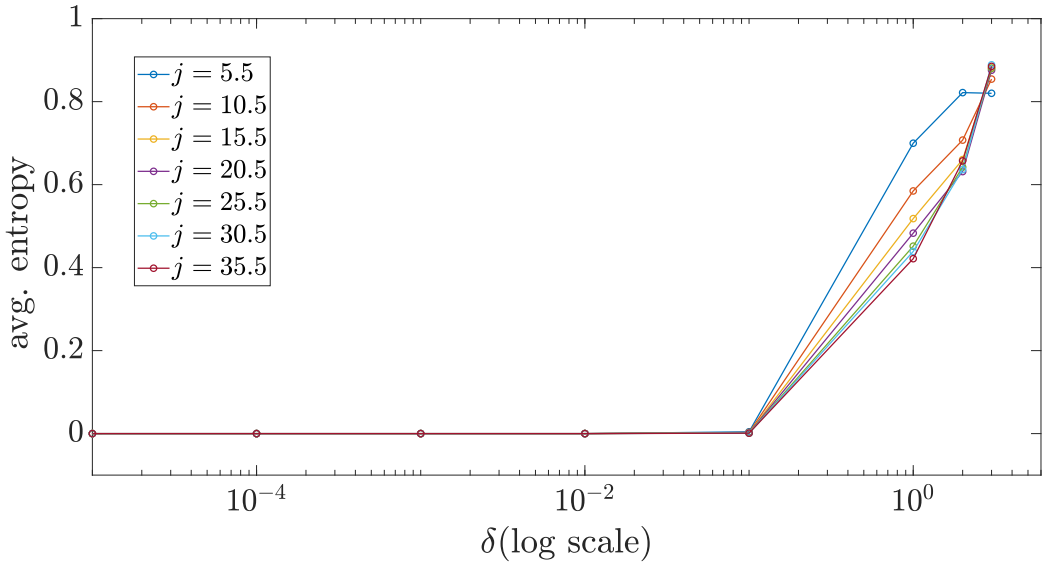

(b)

Figure 4.7: Mean value of time averaged S_{sq} over entire phase with 70 x 140 initial spin coherent states with $\kappa = j\pi + \delta$ and different system sizes. **(a)**. j is integer. Each initial state is time-averaged over 10 applications of $U^{8}_{\pi j+\delta}$. **(b)**. j is half- integer. Each initial state is time-averaged over 10 applications of $U^{12}_{\pi j+\delta}$.

chaos parameter	periodicity	
	Integer spin	Half-integer spin
$\kappa = 0$	4	4
$\kappa = \frac{j\pi}{2}$	48*	NE*
$\kappa = j\pi$	8	12
$\kappa = \frac{3j\pi}{2}$	48*	NE*
$\kappa = 2j\pi$	2	4
$\kappa = \frac{5j\pi}{2}$	48*	NE*
$\kappa = 3j\pi$	8	12
$\kappa = \frac{7j\pi}{2}$	48*	NE*
$\kappa = 4j\pi$	4	4

Table 4.1: Periodicity value for different κ values and $p{=}\frac{\pi}{2}$. Here (*) represents results from numerical simulation and NE signifies the non-existence of periodicity.

We vary δ from 0 to 3 and evolve the initial spin coherent state with $U^T(\kappa+\delta)$, where T is the temporal periodicity and $\kappa = \{2j\pi, j\pi, j\pi/2\}$. Therefore $U^T(\kappa+0) = \mathbb{1}_{2j+1}$ with different values of T for different j and κ value as mentioned in the previous section . The perturbed Floquet unitary is written as

$$\begin{aligned} U^T_{\kappa,\delta} &= \left[\exp\left(-i\frac{\kappa+\delta}{2j}J_z^2\right)\exp\left(-i\frac{\pi}{2}J_y\right)\right]^T, \\ &= \left[\exp\left(-i\frac{\delta}{2j}J_z^2\right)\cdot U_\kappa\right]^T \end{aligned} \tag{4.66}$$

where U_κ is given by Eq. (2.2) with $\kappa = \{2j\pi, j\pi, j\pi/2\}$. To quantify the stability, we used von-Neumann entropy (S_{sq}) of the reduced density matrix of a single qubit. Since we are starting with a spin coherent state, $S_{sq} = 0$ initially. Applying U^T_κ with $\delta = 0$ gives the same state as an initial state. Therefore, there is no generation of entanglement

in the system and S_{sq} remains 0. As we increase δ, S_{sq} becomes non-zero.

Fig 4.6 shows the average S_{sq} for $j = 15.5$, $\kappa = j\pi + \delta$ with different δ values after the action of $U^{mT}(\kappa + \delta)$, where $m \in (0, 10)$. We can see that for low values of δ, there is no distribution to the plot as S_{sq} remains 0. After a certain value, correlations build up in the system but are still very low. On further increasing δ, the system loses its temporal periodicity and shows a high value of S_{sq}, indicating chaotic behavior. Extending this analysis to different system sizes, we calculate the mean value of S_{sq}, over the entire phase space for every δ. We repeat this for different system sizes j. As seen from Fig.4.7a and Fig.4.7b, the value of δ where the system loses its temporal periodicity does not depend on the system size. However, it is different for the integer and half-integer values of j. For $\kappa = j\pi$, an integer value of j, the system loses stability at $\delta = 0.01$, whereas for half-integer value of j, $\delta = 0.1$ is the critical point. It is important to note that with j as a half-integer, the system is one order more stable than for j as an integer value. $\kappa = \frac{j\pi}{2}$ is even more unstable for integer spin, with the critical δ being of order 10^{-3}

This effect of δ can be understood in the following way. Chaos is generated in the quantum kicked top model due to the non-linear part of the Hamiltonian, which depends on twist operator $\exp\left(-i\frac{\kappa}{2j}J_z^2\right)$. The non-linear parts, which are one-axis twisting, create the shearing of the state to create squeezed spin states. This changes the quasi-probability distribution (or Husimi distribution) on the sphere [88]. Here, by shearing, we mean that the state will be stretched and will become delocalized on the sphere. The degree of shearing directly depends on the strength of κ. Since shearing is impulsive, combined with rotation, it destroys the coherent structure of the state and spreads it over the entire sphere. However, at these special values of κ, the non-linear term is unable to create any shearing of the state. Instead, it splits the states and creates a superposition of the split states, as shown in Fig.4.1 and Fig.4.2. As we introduced the perturbation, δ, in the chaoticity parameter (see Eq. (4.66)), the effect of the unitary changes. Although $U_{\delta=0}$ is not able to create shearing, $\exp\left(-i\frac{\delta}{2j}J_z^2\right)$ creates the shearing. However, if δ is not strong enough, then we do not see any shearing as in the case of $\delta < 0.1$ for the half-integer value of j and $\delta < 0.01$ for the integer value of j for a very long time. Once δ is strong enough to create shearing and break the coherent structure

of the state, the system becomes highly delocalized and spreads over the entire phase space. It is surprising to note that for any values of j, the shearing caused by the δ part of the unitary is the same. This is why the critical value of δ, where the system loses stability, is independent of the system's size.

4.4 Discussion

Previous studies regarding the correspondence between classical and quantum dynamics have shown that a chaotic system shows signatures of classical properties in large quantum number limits [4, 38, 34]. A classically chaotic initial state shows exponential growth in quantum correlations, whereas for an initial state centered in regular regions, the growth of quantum correlations is low [33, 67]. This helps to study the chaos in quantum dynamics, whose classical limit is chaotic, and thus Bohr's correspondence was established. In deep quantum regimes, there are studies that show some level of correspondence between the classical phase space and entanglement phase space dynamics [5, 35, 39, 36, 7].

Nevertheless, the transition between classical and quantum dynamics is not plain sailing. Many studies showed that Bohr's correspondence principle breaks down due to the finite size of the Hilbert space [13, 89]. In quantum kicked top, which has a mixed phase space, for a specific parameter, it was shown before that classical instability and initial points that are periodic, show the breakdown of this principle [8]. Bohr's correspondence was quantified in the vicinity of periodic orbits, and a set of criteria was proposed for invoking the correspondence principle. In another work by Lombardi et. al. [9], it was shown that initial states centered at regular points in classical phase space could be entangled more efficiently, breaking the correspondence principle. This suggests that entanglement generation in the kicked top depends on the specific details of the classical dynamics rather than its global properties. In all these works, the breaking of the correspondence principle was shown to be due to system size or the properties of the initial points.

In this chapter, we have discussed a new way of breaking Bohr's correspondence

principle, which depends on the global parameters and is independent of the specific details of classical phase space or quantum number (system size). We have shown that at specific values of κ and p, the system attains temporal periodicity, prohibiting the system from exploring the entire phase space even though classical dynamics at these parameters are entirely chaotic. These temporal periodicities are a unique feature of quantum dynamics and are in addition to the periodicity available due to classical dynamics. The chaos in the quantum evolution of the quantum kicked top is generated due to the non-linear part of the Hamiltonian, whose strength is given by κ, which is also known as one-axis twisting. This creates a shearing of the spin coherent states at the end of every kick. The shearing, along with the rotation, results in chaotic dynamics. However at particular values of κ, the kick part of the unitary is unable to create the shear. It either becomes a rotation, or it splits the state. Therefore, this behavior is the same for all initial spin coherent states. This is contrary to classical dynamics, where periodicity is a property of both parameters and the initial state.

The classical equations of motion are non-linear in nature. The properties of the initial state determine the temporal periodicity along with the system parameters. This can be seen in the kicked-top model. It has a mixed classical phase space where certain regions have regular dynamics, and others have chaotic dynamics for the same values of the parameters. On the other hand, in quantum evolution, being a linear map, the periodicity in the unitary matrix is enough to ensure the repetition of states. Therefore, these periodicities are independent of the initial states and are in addition to the periodicity that arises in classical dynamics due to the effect of parameters and regular orbits.

It should be noted that these present findings do not disprove earlier results about the correspondence between the classical and quantum dynamics in the kicked top. Quantum dynamics of the kicked top resemble classical dynamics in high j limit. Even in the deep quantum regime, the time-averaged entanglement entropy plots show good correspondence with classical phase space dynamics. In Fig. 4.8a, for $\kappa = 2.5$, we have shown the time-averaged entanglement entropy of the reduced density matrix of one qubit for $j = 1$. In the mixed classical phase space for $\kappa = 2.5$, regular initial points correspond to low entanglement entropy, Period-4 points correspond to

high entanglement entropy, and chaotic points correspond to an intermediate value of entanglement entropy. But for $\kappa = \pi$ and $j = 1$, this correspondence does not hold, as shown in Fig. 4.8b. As discussed in the previous section, we recover the classical behavior as we move away from these special values of κ. This is important to note since while studying chaos in a quantum system, such as the kicked-top model, we should be informed about the parameters where classical-quantum correspondence does not hold.

Further work will explore the apparent lack of temporal periodicity in the case of half-integer spin and kick strength in $\kappa = \frac{j\pi}{2}$.

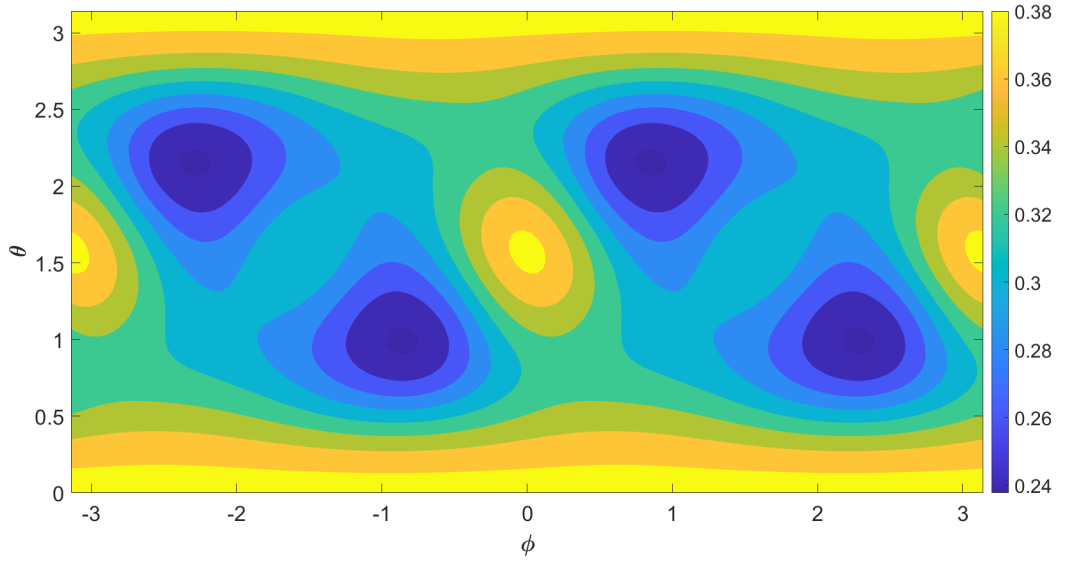

(a)

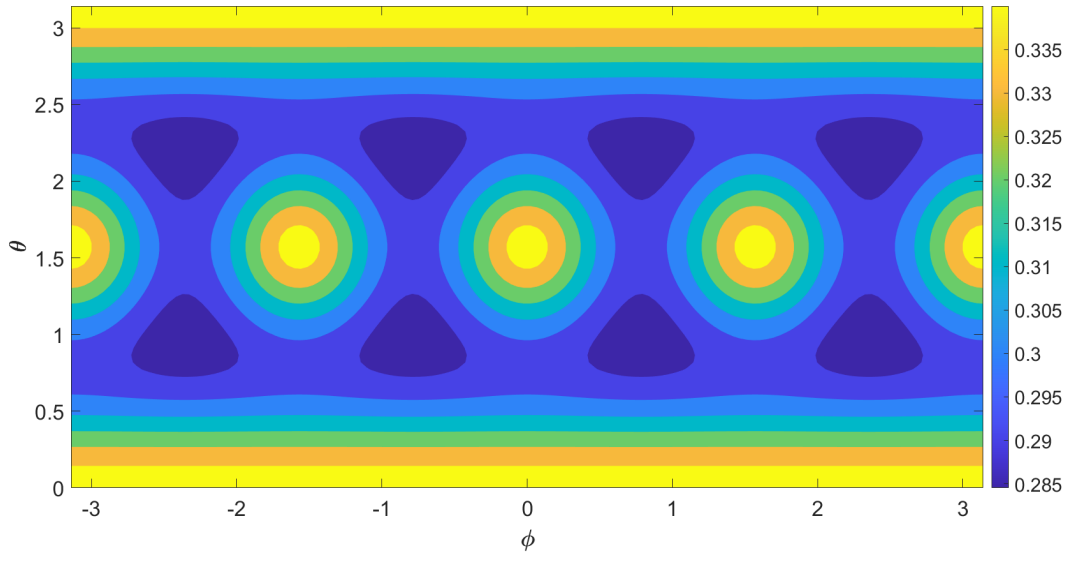

(b)

Figure 4.8: Time averaged S_{sq} over entire phase with 70 x 140 initial spin coherent states for $j = 1$ and. **(a)**. $\kappa = 2.5$ and **(b)**. $\kappa = \pi$.

Chapter 5

Summary and outlook

"An ordered life is a boring life."

This thesis was aimed at the advancement of our understanding of chaos in a quantum system and the quantum-classical correspondence. Quantum theory deals with the linearity, mapping an input to output state, and lacks the important ingredients of classical chaos theory, i.e. non-linearity. However, the existence of models such as the quantum kicked top, which has a chaotic classical limit motivates us to seek the quantum interpretation of chaos.

In our work, we proposed a novel gate-based approach to simulate the chaotic Hamiltonian on currently available Noisy Intermediate Scale Quantum (NISQ) devices chapter 2. We use IBM's 5-qubit open-access quantum computers (Vigo) as the experimental platform to implement the proposed approach for the 2-qubit quantum kicked top [4]. We have constructed and demonstrated an exact simulation for the 2-qubit quantum kicked top using a universal set of quantum logic gates. Our quantum circuit-based simulation is programmable and enables flexible initial state preparation and evolution. We decomposed the unitary evolution operator (U^n) for n kicks, instead of applying the unitary for one time period repeatedly n times; see section 3.2. Therefore there are no systematic errors as we increased the number of kicks. This helps to

explore chaotic dynamics in the regime of an extended range of parameters which was unfeasible to approach with known experiments. Given the high fidelity for a large number of kicks and arbitrary κ values, we have shown the periodicity in quantum correlations (concurrence) as a function of κ; see section 3.4. We have also established a faithful relationship between time average entanglement and classical chaos, two inherent properties of quantum and classical physics respectively as shown in section 3.6. In our study of the 2-qubit QKT, we observed that at $\kappa = j\pi$, the quantum-classical correspondence does not hold. This motivated us to explore the special values of κ in detail in the next chapter.

In the second part of this thesis, chapter 4, first we proved the periodicity of quantum correlations in the chaoticity parameter (κ). Then we analyzed the temporal periodicity of the quantum kicked top for some special values of κ. We showed that for an arbitrary but finite values of integer and half-integer spins for certain values of the parameters (such as κ and p), the entire evolution gets repeated after a certain number of kicks ($U^n = \tau\mathbb{I}$, where τ is some global phase). This restricts the dynamics from exploring the entire phase space and prevents it from showing any chaotic behavior. We proved the exact periodicity for $\kappa = j\pi$, $\kappa = 2j\pi$, and $\kappa = 3j\pi$, for both integer and half-integer spin systems. For the case of integer spin and $\kappa = \frac{mj\pi}{2}$ (where m is odd number $\in \{1,3,5,7\}$), we gave numerical evidence for temporal periodicity. Our numerical simulations led us to conjecture that for half-integer spin and $\kappa = \frac{j\pi}{2}$, temporal periodicity does not exist.

For these special values of the chaoticity parameter (κ), the non-linear part of the unitary i.e., the twist part, splits into a sum of linear operators. Thus, instead of creating a shear, it just splits the state into a superposition of spin coherent states. This prohibits the state to enter chaotic dynamics and thus the quantum-classical correspondence breaks down. This shows that even in the semi-classical regime, for certain values of a parameter, the system never shows any classical behavior i.e., there are no classical analogs of this temporal periodicity. This behavior is independent of the initial location of the state on phase space or system size. There are periodicities in the classical system as well, but those are proprieties of the parameters and initial points on the phase space. It is important to note that classical periodicity still exists in the quantum domain, but in addition, we also get this new periodicity that has no classical counterpart.

We discuss the stability of these recurrences as the κ value is perturbed away and find that some are more stable than others. In all cases however the transition back to "normal" evolution appears to be there. This is confirmed via an analysis of the von Neumann entropy. The stability analysis has an importance of its own. Using the current experimental set-up, we cannot enter the semi-classical regime. In the deep quantum regime, while performing an experiment to study the signatures of classical chaos, it is important to be informed about these special values where correspondence does not hold and one should avoid these special parameters. All together these results suggest a highly intertwined relationship between the chaoticity periodicity structure and the temporal periodicity structure. Nevertheless, it implies an interesting challenge to the correspondence principle as these recurrences exist in all finite dimensions. Observing these phenomena in a physical set-up requires separate experimental studies of its own.

The utmost goal of the field of "quantum chaos" is to develop a definition of chaos in quantum systems [69, 90, 62]. To achieve this goal, we need to have an explicit understanding of the transition from quantum to classical systems. This is essential since any new complete theory should be able to reproduce the results of an existing theory [3]. Therefore, any theory of quantum chaos should incorporate classical chaos in some appropriate conditions. The work done in this thesis is focused on exploring the above-mentioned relationship between the old and new theory i.e. classical and quantum respectively. By efficiently implementing the 2-qubit QKT on a quantum computer, we show that one can recover classical phase space dynamics through the entanglement dynamics even in a deep quantum regime. However, whether this correspondence between classical and quantum dynamics holds for all conditions is investigated in the second half of the thesis.

The two main results of this thesis complement each other. One indicates correspondence in a deep quantum regime while the other shows a breakdown of the same even in a semi-classical regime for special parameters of the Hamiltonian. This suggests that the quantum-classical transition is not simple. For a given parameter, on increasing the quantum numbers j, the system shows a breakdown of Bohr's correspondence principle on multiple occasions before attaining the classical limit. One natural question that arises from our study is since the quantum-classical

correspondence does not hold for many parameter settings, should we abandon this approach of studying chaos in quantum systems? This question can be answered in the following ways: Even though the correspondence does not hold for all parameter values, it does hold in many situations. Since we do not have any proper definition of "quantum chaos", we should continue with this approach of using classical chaos as a reference. Once we develop a base definition of "quantum chaos", we can proceed with a different approach where we also study the system independent of its classical limit.

5.1 Future work

There are several ways work done in this thesis can be extended in the future. The hybrid approach of classical processing and quantum computation enables us to reach a new degree of experimental capability. One can develop an efficient way of decomposing a unitary by using its symmetry and scaling it for a large number of qubits. This will also help in studying different dynamical properties (such as bifurcation), which are more prominent in the semi-classical regime [8]. If scalable, then the current system can also be used for the bench-marking of quantum computers. One such study to use chaos for bench marking of quantum computers is shown in [91]. This method can also be used to generate a state with a variable degree of entanglement.

Another natural extension is to prove the non-periodicity for half-integer spin and κ as odd multiples of $\frac{j\pi}{2}$. It is interesting to note that for j=3/2, the Hilbert space is 4-dimensional. Even in low-dimension space, numerical simulations suggest that the dynamics is non-periodic. Another possible extension is to study the entire spectrum of κ values and find a general expression for the different parameters where the dynamics show temporal periodicity. Once these results are established, this method can be applied to a different model where we can see the similar behavior.

References

[1] M. C. Gutzwiller. *Chaos in Classical and Quantum Mechanics*. Springer New York, 1990.

[2] F. Haake. Quantum signatures of chaos. In *Quantum Coherence in Mesoscopic Systems*, pages 583–595. Springer, 1991.

[3] N. Bohr. ber die serienspektra der elemente. 2:423–469, 10 1920.

[4] F. Haake, M. Kuś, and R. Scharf. Classical and quantum chaos for a kicked top. *Zeitschrift für Physik B Condensed Matter*, 65:381–395, 09 1987.

[5] V. R. Krithika, V. S. Anjusha, Udaysinh T. Bhosale, and T. S. Mahesh. Nmr studies of quantum chaos in a two-qubit kicked top. *Phys. Rev. E*, 99:032219, Mar 2019.

[6] S. Ghose, R. Stock, P. Jessen, R. Lal, and A. Silberfarb. Chaos, entanglement, and decoherence in the quantum kicked top. *Physical Review A*, 78(4):042318, 2008.

[7] C. Neill, P. Roushan, M. Fang, Y. Chen, M. Kolodrubetz, Z. Chen, A. Megrant, R. Barends, B. Campbell, B. Chiaro, et al. Ergodic dynamics and thermalization in an isolated quantum system. *Nature Physics*, 12(11):1037–1041, 2016.

[8] M. Kumari and S. Ghose. Quantum-classical correspondence in the vicinity of periodic orbits. *Phys. Rev. E*, 97:052209, May 2018.

[9] M. Lombardi and A. Matzkin. Entanglement and chaos in the kicked top. *Physical Review E*, 83, 01 2011.

[10] R. P Feynman, R. B Leighton, and M. Sands. *The Feynman lectures on physics : commemorative issue. Vol. 3*. Addison-Wesley, 1989.

[11] P. Ehrenfest. Bemerkung ber die angen herte g ltigkeit der klassischen mechanik innerhalb der quantenmechanik. *Zeitschrift f r Physik*, 45:455–457, 07 1927.

[12] J. Wisdom. Urey prize lecture: Chaotic dynamics in the solar system. *Icarus*, 72:241–275, 11 1987.

[13] W. H Zurek and Juan P. P. Quantum chaos: a decoherent definition. 83:300–308, 05 1995.

[14] W. H Zurek and Juan P. P. Why we don't need quantum planetary dynamics: Decoherence and the correspondence principle for chaotic systems. pages 167–177, 01 1999.

[15] J. E Ford, G. Mantica, and G. H. Ristow. The arnol'd cat: Failure of the correspondence principle. 50:493–520, 08 1991.

[16] J. Ford and G. Mantica. Does quantum mechanics obey the correspondence principle? is it complete? *American Journal of Physics*, 60:1086–1098, 12 1992.

[17] J. Ford and M. Ilg. Eigenfunctions, eigenvalues, and time evolution of finite, bounded, undriven, quantum systems are not chaotic. *Phys. Rev. A*, 45:6165–6173, May 1992.

[18] V. I. Arnold. *Mathematical Methods of Classical Mechanics*. Springer New York, 1989.

[19] S. H. Strogatz. *Nonlinear Dynamics and Chaos: With Applications to Physics, Biology, Chemistry and Engineering*. Westview Press, 2000.

[20] A. Peres. Stability of quantum motion in chaotic and regular systems. *Phys. Rev. A*, 30:1610–1615, Oct 1984.

[21] Rüdiger Schack, G. M. D'Ariano, and C. M. Caves. Hypersensitivity to perturbation in the quantum kicked top. *Phys. Rev. E*, 50:972–987, Aug 1994.

[22] T. ž Prosen. General relation between quantum ergodicity and fidelity of quantum dynamics. *Phys. Rev. E*, 65:036208, Feb 2002.

[23] M. F. Andersen, A. Kaplan, T. Grünzweig, and N. Davidson. Decay of quantum correlations in atom optics billiards with chaotic and mixed dynamics. *Phys. Rev. Lett.*, 97:104102, Sep 2006.

[24] J. Maldacena, S. H. Shenker, and D. Stanford. A bound on chaos. *Journal of High Energy Physics*, 2016, 08 2016.

[25] K. Hashimoto, K. Murata, and R. Yoshii. Out-of-time-order correlators in quantum mechanics. 2017, 03 2017.

[26] B. Swingle and D. Chowdhury. Slow scrambling in disordered quantum systems. *Phys. Rev. B*, 95:060201, Feb 2017.

[27] E. B. Rozenbaum, L. A. Bunimovich, and V. M. Galitski. Quantum chaos in classically non-chaotic systems. *arXiv: Quantum Physics*, 2019.

[28] T. Xu, T. Scaffidi, and X. Cao. Does scrambling equal chaos? *Phys. Rev. Lett.*, 124:140602, Apr 2020.

[29] R. Horodecki, P. Horodecki, M. Horodecki, and K. Horodecki. Quantum entanglement. *Rev. Mod. Phys.*, 81:865–942, Jun 2009.

[30] K. Furuya, M. C. Nemes, and G. Q. Pellegrino. Quantum dynamical manifestation of chaotic behavior in the process of entanglement. *Phys. Rev. Lett.*, 80:5524–5527, Jun 1998.

[31] R. M. Angelo, K. Furuya, M. C. Nemes, and G. Q. Pellegrino. Rapid decoherence in integrable systems: A border effect. *Phys. Rev. E*, 60:5407–5411, Nov 1999.

[32] R. M. Angelo, K. Furuya, M. C. Nemes, and G. Q. Pellegrino. Recoherence in the entanglement dynamics and classical orbits in the n-atom jaynes-cummings model. *Phys. Rev. A*, 64:043801, Sep 2001.

[33] S. Ghose, C. R. Paul, and R. Stock. Quantum chaos and tunneling in the kicked top. *laser Physics*, 18:1098–1105, Sep 2007.

[34] S. Ghose and B. sanders. Entanglement dynamics in chaotic system. *Phys. Rev. A*, 70:062315, Dec 2004.

[35] J. B. Ruebeck, J. Lin, and A. K Pattanayak. Entanglement and its relationship to classical dynamics. *Physical Review E*, 95(6):062222, 2017.

[36] U. T. Bhosale and M. S. Santhanam. Periodicity of quantum correlations in the quantum kicked top. *Phys. Rev. E*, 98:052228, Nov 2018.

[37] V. Madhok, S. Dogra, and A. Lakshminarayan. Quantum correlations as probes of chaos and ergodicity. *Optics Communications*, 420:189–193, Aug 2018.

[38] S. Dogra, V. Madhok, and A. Lakshminarayan. Quantum signatures of chaos, thermalization, and tunneling in the exactly solvable few-body kicked top. *Phys. Rev. E*, 99:062217, Jun 2019.

[39] A. Anand, S. Srivastava, S. Gangopadhyay, and S. Ghose. Simulating quantum chaos on a quantum computer. *arXiv preprint arXiv:2107.09809*, 2021.

[40] R. P. Feynman. Simulating physics with computers. *International Journal of Theoretical Physics*, 21:467–488, 06 1982.

[41] I. M. Georgescu, S. Ashhab, and Franco Nori. Quantum simulation. *Rev. Mod. Phys.*, 86:153–185, Mar 2014.

[42] S. Lloyd. Universal quantum simulators. *Science*, 273:1073–1078, 08 1996.

[43] K. Bharti, A. Cervera-Lierta, T. H. Kyaw, T. Haug, S. Alperin-Lea, A. Anand, M. Degroote, H. Heimonen, J. S. Kottmann, T. Menke, Wai-Keong Mok, S. Sim, Leong-Chuan Kwek, and A. Aspuru-Guzik. Noisy intermediate-scale quantum algorithms. *Rev. Mod. Phys.*, 94:015004, Feb 2022.

[44] J. Preskill. Quantum computing in the nisq era and beyond. *Quantum*, 2:79, 08 2018.

[45] IBM Quantum team. Retrieved from ibmq_vigo v1.0.2 (2020).

[46] J. M. Radcliffe. Some properties of coherent spin states. *Journal of Physics A: General Physics*, 4:313–323, 05 1971.

[47] J. Ma, X. Wang, C.P. Sun, and F. Nori. Quantum spin squeezing. *Physics Reports*, 509:89–165, 12 2011.

[48] G. S. Agarwal. Relation between atomic coherent-state representation, state multipoles, and generalized phase-space distributions. *Phys. Rev. A*, 24:2889–2896, Dec 1981.

[49] H. Fan, K. Matsumoto, and H. Imai. Quantify entanglement by concurrence hierarchy. *Journal of Physics A: Mathematical and General*, 36:4151–4158, 03 2003.

[50] W. K. Wootters. Entanglement of formation of an arbitrary state of two qubits. *Phys. Rev. Lett.*, 80:2245–2248, Mar 1998.

[51] S. Bettelli and D. L. Shepelyansky. Entanglement versus relaxation and decoherence in a quantum algorithm for quantum chaos. *Phys. Rev. A*, 67:054303, May 2003.

[52] X. Wang, S. Ghose, B. C. Sanders, and B. Hu. Entanglement as a signature of quantum chaos. *Physical Review E*, 70(1):016217, 2004.

[53] C. H. Bennett, H. J. Bernstein, S. Popescu, and B. Schumacher. Concentrating partial entanglement by local operations. *Phys. Rev. A*, 53:2046–2052, Apr 1996.

[54] Tzu-Chieh Wei and P. M. Goldbart. Geometric measure of entanglement and applications to bipartite and multipartite quantum states. *Phys. Rev. A*, 68:042307, Oct 2003.

[55] A. Shimony. Degree of entanglement. *Annals of the New York Academy of Sciences*, 755:675–679, 04 1995.

[56] R. Hübener, M. Kleinmann, T. Wei, C. González-Guillén, and O. Gühne. Geometric measure of entanglement for symmetric states. *Phys. Rev. A*, 80:032324, Sep 2009.

[57] C. S. Malcolm. The general problem of the stability of motion : Translated and edited by a. t. fuller. taylor and francis, 1992. *Autom.*, 31:353–354, 1995.

[58] E. Ott. Chaos in dynamical systems, Aug 2002.

[59] B. N. Datta. *Stability, Inertia, and Robust Stability*, page 201–243. Elsevier, 2004.

[60] B. Georgeot and D. L. Shepelyansky. Quantum chaos border for quantum computing. *Phys. Rev. E*, 62:3504–3507, Sep 2000.

[61] B. Georgeot and D. L. Shepelyansky. Emergence of quantum chaos in the quantum computer core and how to manage it. *Phys. Rev. E*, 62:6366–6375, Nov 2000.

[62] S. Ghose. Quantum and classical dynamics of atoms in a magneto-optical lattice. In *AIP Conference Proceedings*. AIP, 2003.

[63] I. M. Georgescu, S. Ashhab, and F. Nori. Quantum simulation. *Rev. Mod. Phys.*, 86:153–185, Mar 2014.

[64] S. McArdle, S. Endo, A. Aspuru-Guzik, S. C. Benjamin, and X. Yuan. Quantum computational chemistry. *Reviews of Modern Physics*, 92(1), Mar 2020.

[65] J. Li, R. Fan, H. Wang, B. Ye, B. Zeng, H. Zhai, X. Peng, and J. Du. Measuring out-of-time-order correlators on a nuclear magnetic resonance quantum simulator. *Physical Review X*, 7(3), Jul 2017.

[66] P. Szriftgiser, H. Lignier, J. Ringot, J. C. Garreau, and D. Delande. Experimental study of quantum chaos with cold atoms. *Communications in Nonlinear Science and Numerical Simulation*, 8(3–4):301–313, Sep 2003.

[67] S. Chaudhury, A. Smith, B.E. Anderson, S. Ghose, and P. S. Jessen. Quantum signatures of chaos in a kicked top. *Nature*, 461(7265):768–771, 2009.

[68] V. Madhok, V. Gupta, D. A. Trottier, and S. Ghose. Signatures of chaos in the dynamics of quantum discord. *Phys. Rev. E*, 91:032906, Mar 2015.

[69] M. Kumari. Quantum-classical correspondence and entanglement in periodically driven spin systems. *Uwaterloo.ca*, 07 2019.

[70] Chi-K. Li and D. Pelejo. Decomposition of quantum gates. *arXiv:1311.3599 [quant-ph]*, 12 2013.

[71] A. Barenco, C. H. Bennett, R. Cleve, D. P. DiVincenzo, N. Margolus, P. Shor, T. Sleator, J. A. Smolin, and H. Weinfurter. Elementary gates for quantum computation. *Phys. Rev. A*, 52:3457–3467, Nov 1995.

[72] Qiskit 0.23.2 documentation — qiskit 0.23.2 documentation.

[73] *Qiskit: An Open-source Framework for Quantum Computing*.

[74] S. Nishio, Y. Pan, T. Satoh, H. Amano, and R. Van Meter. Extracting success from ibm's 20-qubit machines using error-aware compilation. *ACM Journal on Emerging Technologies in Computing Systems*, 16:1–25, 07 2020.

[75] G. García-Pérez, M. A C Rossi, and S. Maniscalco. Ibm q experience as a versatile experimental testbed for simulating open quantum systems. *npj Quantum Information*, 6(1):1–10, 2020.

[76] L. Viola and S. Lloyd. Dynamical suppression of decoherence in two-state quantum systems. *Physical Review A*, 58(4):2733–2744, Oct 1998.

[77] C. Berke, E. Varvelis, S. Trebst, A. Altland, and D. DiVincenzo. Transmon platform for quantum computing challenged by chaotic fluctuations. *arXiv: Quantum Physics*, 2020.

[78] J. R. Nielsen. *The Correspondence Principle (1918-1923)*. Elsevier, 1976.

[79] J. Wilkie and P. Brumer. Quantum-classical correspondence via liouville dynamics. i. integrable systems and the chaotic spectral decomposition. *Physical Review A*, 55:27–42, 01 1997.

[80] J. Wilkie and P. Brumer. Quantum-classical correspondence via liouville dynamics. ii. correspondence for chaotic hamiltonian systems. *Physical Review A*, 55:43–61, 01 1997.

[81] S. Fortin and O. Lombardi. The correspondence principle and the understanding of decoherence. *Foundations of Physics*, 49:1372–1393, 11 2019.

[82] E. J. Meier, J. Ang'ong'a, F. A. An, and B. Gadway. Exploring quantum signatures of chaos on a floquet synthetic lattice. *Phys. Rev. A*, 100:013623, Jul 2019.

[83] Z. Zou and J. Wang. Pseudoclassical dynamics of the kicked top. *Entropy*, 24(8):1092, Aug 2022.

[84] F. M. Izrailev and D. L. Shepelyanskii. Quantum resonance for a rotator in a nonlinear periodic field. *Theoretical and Mathematical Physics*, 43(3):553–561, Jun 1980.

[85] F. M. Izrailev and D. L. Shepelyanskii. Quantum resonance for a rotator in a nonlinear periodic field. *Theoretical and Mathematical Physics*, 43:553–561, 06 1980.

[86] J. F. Kanem, S. Maneshi, M. Partlow, M. Spanner, and A. M. Steinberg. Observation of high-order quantum resonances in the kicked rotor. *Physical Review Letters*, 98, 02 2007.

[87] A. W Harrow. The church of the symmetric subspace. *arXiv preprint arXiv:1308.6595*, 2013.

[88] M. Kitagawa and M. Ueda. Squeezed spin states. *Physical Review A*, 47:5138–5143, 06 1993.

[89] W. H. Zurek and J. P. Paz. Decoherence, chaos, and the second law. *Phys. Rev. Lett.*, 72:2508–2511, Apr 1994.

[90] J. Emerson. Quantum chaos and quantum-classical correspondence. *arXiv preprint quant-ph/0211035*, 2002.

[91] J. Harris, B. Yan, and N. A. Sinitsyn. Benchmarking information scrambling. *PRL*, 129, 10 2021.

[92] A. Peres. *Quantum theory: concepts and methods*, volume 57. Springer Science & Business Media, 2006.

[93] J. I. Cirac and P. Zoller. Goals and opportunities in quantum simulation. *Nature Physics*, 8(4):264–266, Apr 2012.

[94] R. P. Feynman. Quantum mechanical computers. *Foundations of Physics*, 16(6):507–531, Jun 1986.

[95] E. Altman, K. R. Brown, G. Carleo, L. D. Carr, E. Demler, C. Chin, B. DeMarco, S. E. Economou, M. A. Eriksson, Kai-Mei C. Fu, and et al. Quantum simulators: Architectures and opportunities. *PRX Quantum*, 2(1), Feb 2021.

[96] S. Leontica, F. Tennie, and T. Farrow. Simulating molecules on a cloud-based 5-qubit ibm-q universal quantum computer. *Communications Physics*, 4, 06 2021.

[97] M. A. C. García-Pérez, G.and Rossi and S. Maniscalco. Ibm q experience as a versatile experimental testbed for simulating open quantum systems. *npj Quantum Information*, 6, 01 2020.

[98] G. Casati, B. V. Chirikov, F. M. Izraelev, and J. Ford. *Stochastic behavior of a quantum pendulum under a periodic perturbation*, volume 93 of *Lecture Notes in Physics*, page 334–352. Springer-Verlag, Berlin/Heidelberg, 1979.

[99] S. Fishman, D. R. Grempel, and R. E. Prange. Chaos, quantum recurrences, and anderson localization. *Phys. Rev. Lett.*, 49:509–512, Aug 1982.

[100] G. Casati and I. Guarneri. Non-recurrent behaviour in quantum dynamics. *Communications in Mathematical Physics*, 95(1):121–127, Mar 1984.

[101] J. W. Z. Lau, K. H. Lim, H. Shrotriya, and L. C. Kwek. Nisq computing: where are we and where do we go? *AAPPS Bulletin*, 32, 09 2022.

[102] M. Blasone, F. Dell'Anno, S. De Siena, and F. Illuminati. Hierarchies of geometric entanglement. *Phys. Rev. A*, 77:062304, Jun 2008.

[103] P P Kulish and Nicolai R. Quantum linear problem for the sine-gordon equation and higher representations. 23:2435–2441, 01 1983.